INVESTIGATION OF THE $Li^6(p, n)Be^6$ REACTION BY THE NEUTRON THRESHOLD TECHNIQUE

Thesis by
John Leonard Honsaker

In Partial Fulfillment of the Requirements
For the Degree of
Doctor of Philosophy

California Institute of Technology
Pasadena, California
1965
(Submitted November 2, 1964)

ACKNOWLEDGEMENTS

It is a pleasure to thank the faculty, staff, and graduate students of the W. K. Kellogg Radiation Laboratory for their kind assistance during the course of this work. Gratitude is particularly expressed to Professors T. Lauritsen and W. A. Fowler for suggesting the problem and for their continuing guidance. To Dr. T. A. Tombrello, special thanks are due for many discussions which were indispensable to the analysis of the data, and also for the Coulomb wave function program which he made available. Professor W. Whaling and Mr. W. D. Harrison kindly communicated their experimental results prior to publication. The author also wishes to thank Barbara Zimmerman for advice about the computer programming and help in preparing the figures, and he is especially grateful to his wife, Leni, for constant encouragement and assistance during the writing.

Thanks are also expressed to the California Institute of Technology and the National Science Foundation for financial assistance in the form of scholarships, fellowships, and assistantships during the course of graduate study. The research project was supported by the joint program of the Office of Naval Research and the U. S. Atomic Energy Commission.

ABSTRACT

This thesis describes the measurement of the reaction $Li^6(p,n)Be^6$ by slow-neutron methods, with particular attention to the Be^6 ground-state threshold. The detector response was calculated by a Monte Carlo technique and verified with a measurement of the $Li^7(\alpha,n)B^{10}$ threshold. An analysis of the shape of the Be^6 threshold indicated that both s- and p-wave neutrons contribute significantly to the reaction. The results depend on what mode of decay is assumed for the ground state of Be^6. If a two-stage process is assumed, with either an alpha particle and an unbound diproton or Li^5 and a proton as intermediate state, the width is found to be 95 ± 28 keV and the Q-value obtained for the $Li^6(p,n)Be^6$ reaction is -5074 ± 13 keV. It was not possible to determine which process is predominant. No further states in Be^6 with excitation energy less than 4 MeV and width less than 1.5 MeV could be detected. Evidence suggesting other neutron-producing reactions from the proton bombardment of Li^6 at higher energies is discussed.

TABLE OF CONTENTS

I. INTRODUCTION

1. The Be^6 Ground State

One aspect of the problem of the structure of light nuclei concerns the characteristics of a system containing a small number of particles interacting by nuclear forces. The nuclei of mass 6, He^6, Li^6 and Be^6, in their states of lowest energy may be considered as systems of three particles: two nucleons and an alpha particle, the latter not subject to internal disruption because of its tight binding.

The least studied of these mass 6 isobars is Be^6, which is distinguished from the others in being unstable in its ground state against breakup into its three constituents (Ajzenberg-Selove and Lauritsen, 1962). The He^6 ground state is stable except for beta-decay to Li^6.

The 3.56 MeV state in Li^6, which is analogous to the ground states of the other two nuclei, decays electromagnetically. Its spin and parity (0^+) forbid decay by emission of a deuteron.

Be^6 can be formed as a product of the reaction $Li^6(p, n)Be^6$. The energy relationships for this reaction and the various other products which can be formed by bombardment of Li^6 with protons are shown in Figure 1 for the appropriate region of total energy.

Consider the detailed mechanism of the decay of Be^6. The final state inevitably consists of an alpha particle and two free protons. Thus, it may nominally be classified as a three-body breakup. However, closer consideration indicates that the interaction between two of the particles is very likely to be stronger than between either one of these and the third particle. An equality in the strengths of the three possible interactions is extremely improbable unless the particles are identical, as for example $C^{12} \rightarrow 3\,\alpha$. It seems, therefore, reasonable to approximate the decay by a series of two-body decays. Because of the two identical protons involved in this case, two of the three possible decay sequences are the same, so only two distinct modes need be treated.

If the first stage of decay is the emission of either of the protons, then the stronger forces must be between alpha and proton. These form an intermediate residual state, otherwise known as Li^5. In the region of energy involved here, α + p scattering experiments indicate a p-wave resonance which is the ground state of Li^5. Although the resonance energy lies above the energy available from the decay of Be^6, the width of Li^5 means that final states of the Li^5 + p system exist which conserve energy.

If the alpha particle is the first to be emitted, the forces between the proton pair must dominate. The low energy p + p scattering data can be used to indicate the nature of the intermediate residual state for this case.

If the time interval between successive decays is sufficiently short, the decay sequences cannot be distinguished. This case was not considered in the following analysis. Because the relative kinetic energies of the three particles are not very large, one expects the final state interactions to have some degree of importance in this case as well as in the others.

2. Previous Results

All previously reported observations of the Be^6 ground state have made use of the reaction $Li^6(p,n)Be^6$. These experiments employed three different techniques of neutron spectroscopy. The first production of Be^6 was reported by Bogdanov et al., (1957), using a cyclotron with proton energy 9.6 MeV. The time-of-flight spectrum of neutrons from the reaction indicated an energy group corresponding to the Be^6 ground state. The experiment has been repeated using the same method, but with better resolution, by Gulyamov et al., (1963). At 9.96 MeV proton energy, their Q-value to the ground state is $-5.08 \pm .04$ MeV, and they obtain a width of $0.14 \pm .04$ MeV.

Ajzenberg-Selove et al., (1959) measured neutron groups from the same reaction at $E_p = 10.5$ MeV, using proton recoil tracks in nuclear emulsion for determining the neutron energies. They made measurements at four

If the time interval between successive decays is sufficiently short, the decay sequences cannot be distinguished. This case was not considered in the following analysis. Because the relative kinetic energies of the three particles are not very large, one expects the final state interactions to have some degree of importance in this case as well as in the others.

2. Previous Results

All previously reported observations of the Be^6 ground state have made use of the reaction $Li^6(p,n)Be^6$. These experiments employed three different techniques of neutron spectroscopy. The first production of Be^6 was reported by Bogdanov et al., (1957), using a cyclotron with proton energy 9.6 MeV. The time-of-flight spectrum of neutrons from the reaction indicated an energy group corresponding to the Be^6 ground state. The experiment has been repeated using the same method, but with better resolution, by Gulyamov et al., (1963). At 9.96 MeV proton energy, their Q-value to the ground state is $-5.08 \pm .04$ MeV, and they obtain a width of $0.14 \pm .04$ MeV.

Ajzenberg-Selove et al., (1959) measured neutron groups from the same reaction at $E_p = 10.5$ MeV, using proton recoil tracks in nuclear emulsion for determining the neutron energies. They made measurements at four

angles, finding a ground-state group in each case. The Q-value is given as -5.05 ± .2 MeV. In addition, one neutron group was measured on the plate at 90^{o} which would correspond to an excited state in Be^{6} at 1.5 MeV. The level was estimated to be < 100 keV wide. From the data presented, the intensity seems to be about 1/4 that of the ground-state group.

Another measurement of this reaction was done by Freeman and West (1962), using a He^{3} ionization chamber as neutron spectrometer. The pulse heights of $He^{3}(n, p)H^{3}$ reactions were measured. For E_{p} = 6.6 MeV, they observed a ground-state neutron group, yielding the values Q = -5.061 ± .017 MeV and level width 126 ± 15 keV.

3. Threshold Measurements

A measurement independent of these spectroscopic methods utilizes the behavior of nuclear reactions at a threshold. For any reaction having a negative Q-value, the threshold is simply the lowest bombarding energy for which the reaction can take place. If the reaction products all have a definite mass, it will be impossible to observe them when the beam energy is less than the threshold energy. A discontinuous rise in the number of reaction products can be observed as the bombarding energy increases above threshold, provided that the products are all stable and that there is no energy-dependent interaction between them.

The presence of a potential barrier inhibiting the separation of the reaction products will eliminate the abrupt rise expected in the case of no interaction (Blatt and Weisskopf, 1952). When there are two or more charged particles from the reaction, the Coulomb barrier must be penetrated at threshold, since particles with finite mass must separate with zero kinetic energy in the center-of-mass system at threshold. When the spins of the reaction products are such as to require nonzero orbital angular momentum among them, an effective centrifugal barrier causes a similar result. In these cases, the slope of the yield curve is zero at threshold, and increases gradually with bombarding energy. This means that the threshold energy cannot be measured directly.

The case of s-wave neutrons produced in conjunction with a single residual nucleus satisfies the criteria for a sharp rise in the yield curve at threshold. Measurements of such sharp thresholds have often been used to obtain Q-values for (p, n) and other reactions (Bonner, 1960). Conversely, reactions with well-known neutron thresholds are often used to calibrate the energy scale of accelerator beam-analyzing apparatus (Marion, 1961). The reaction $Li^7(p, n)Be^7$ is especially suited to this purpose, since its threshold has been very accurately measured using absolute electrostatic and precision magnetic analyzers.

This property of neutron thresholds can also be used to obtain information about the lifetime of the residual nucleus. In the case of spectroscopy of neutrons or charged particles, one observes the increase in width of an energy group due to the lifetime of the final state. The limitation is the resolution of the apparatus, for which the ideal response would be a delta function with respect to the energy of the observed particle. The threshold method, on the other hand, ideally has a perfectly sharp discontinuity in the slope of the reaction yield as a function of bombarding energy, and any rounding of the sharp corner could be attributed to an energy spread due to the finite lifetime of the reaction products. The initial particles must have lifetimes too long to have a measurable effect in any practical case.

In an experimental situation, other factors may cause the rounding of an ideal sharp corner at threshold. These limit the resolution for measuring level widths, but can ordinarily be kept down to a small effect. One of these is the spread of incident energies because of the finite resolution of the beam analyzer. Another is the energy loss of particles in penetrating the target layer. The energy interval above threshold which has a rounding of the threshold curve due to these causes can be kept within a few keV, as will be discussed in Part IV. Thermal motion of the target nuclei has a much smaller effect, and may be entirely neglected.

Measurement of a reaction near threshold means that the particles produced have small relative velocities. As this is equivalent to the condition that a relatively long time is required for the decay process to occur, the compound nucleus description of reactions which is based on this condition seems to be the most applicable. A description in terms of the direct-interaction scheme would be valid only when the total energy is sufficiently far above threshold that the relative velocity of the decay products is comparable to motion within the nuclear potential.

The relative importance of the neutron partial waves has additional significance for thresholds broadened by the product state. If a sharp threshold is being measured, only s-waves need be considered in the first few kilovolts above threshold. Higher orbital angular momenta do not appear because the neutrons have too little energy in the center-of-mass system to penetrate the centrifugal barrier. In the case of a broadened threshold, neutrons produced at a given bombarding energy are not restricted to a definite energy, but are distributed in a spectrum whose shape depends on the final state of the residual nucleus. Some higher energy neutrons are produced, no matter how close one is to the "threshold energy", and higher ℓ -values cannot be neglected. Since the higher energy neutrons leave the residual state in the tail of its distribution, their intensity decreases with increasing energy. In general, there may be maxima corresponding to other unstable residual states, and there will always be an upper limit to the neutron energy corresponding to a stable final state.

The centrifugal barrier height,

$$E_{cb} = \ell(\ell+1)\hbar^2/2\mu R^2 \quad ,$$

inhibits the partial waves more strongly with increasing ℓ. However, the partial waves are not necessarily ordered in strength according to ℓ. The compound nucleus may be characterized by resonances, and the relation between their spins and parities and those of the residual state can determine the partial waves which predominate. Thus, the situation is considerably more complicated than in the case of a sharp threshold.

II. EXPERIMENTAL APPARATUS

1. Targets

Since the neutrons are all traveling in the forward direction when the bombarding energy is slightly above threshold, the detector must be placed in line with the incident beam. In the case of beam energies high enough to produce neutrons from any target backing material this is a disadvantage, since one cannot use thin foil targets and dispose of the unused beam at a large distance from the detector. Studies of the neutron-producing properties of suitable backing materials have been made (Bromley et al., 1959). The materials giving lowest background have either a high atomic number and thus a large Coulomb barrier, or have an unusually large negative Q for the background producing reaction.

Gold was chosen as the material for target backing and beam collimator because it offers several advantages. Its neutron production is one of the lowest for protons of around 6 MeV, it is easily obtainable in pure form, easily formable, and has a very large thermal conductivity. The latter is quite important, since the low melting point of lithium would create difficulties if the target were allowed to heat under bombardment.

The target backing was made from 0.05 cm thick gold sheet which had been polished to a mirror finish. Two such sheets were mounted back to back on a copper block attached to a copper rod which was inserted into the target chamber. By rotating the rod 180° it was possible to exchange the positions of the two gold blanks exactly. Stops on the rod holder guaranteed that the original angle

and the reversed position could be reproduced as often as necessary. The gold extended past the end of the copper block so that neutrons emitted in the forward direction had only to penetrate two thicknesses of gold and the glass wall of the target chamber before entering the detector system.

Lithium was evaporated onto one side of the target assembly in a vacuum system directly connected to the target chamber, so that the targets could be made and bombarded without being exposed to the air. The target blank on the other side was used for background measurement. When the targets were eventually removed, it was found that most of the lithium could easily be washed off, but a small amount diffused into the gold and could only be removed by polishing. This means that the lithium density was not completely uniform through the target layer. To minimize this effect, the diffused lithium-gold surface was carefully cleaned off before a fresh target was made.

2. Threshold Detector System

The threshold neutrons were detected by means of a scintillator containing boron and ZnS(Ag) in an intimate mixture. The boron, enriched to 96% B^{10}, captures neutrons through the reaction $B^{10}(n, \alpha)Li^{7}$. The reaction is exoergic, releasing 2.31 or 2.79 MeV into kinetic energy of the charged products, depending on whether the ground state or the first excited state of Li^{7} is formed. The energetic products stimulate nearby ZnS crystals to emit light, which is partially reabsorbed before passing through a 1.27 cm lucite light pipe to a type 6342 photomultiplier. Because of the reabsorption in the ZnS, the pulse height output of the photo-

multiplier does not resolve the two energy groups produced by monoenergetic incident neutrons, but shows a continuous distribution which decreases gradually to zero at the pulse height corresponding to the full energy from the reaction.

Pulses from the photomultiplier were amplified by an integrating preamplifier of standard design and a Hamner Model N-328 double-delay-line amplifier and discriminator circuit. Amplified pulses which exceeded the adjustable discriminator level triggered standard pulses which were registered in an Eldorado Model SC-700 scaler.

The sensitive layer was 0.3 mm thick and 5.08 cm in diameter, with a thin white reflector on the side facing the target. The detector, light pipe and reflector were manufactured by Nuclear Enterprises Ltd., Winnipeg, Canada (type NE-402). The thin scintillator effectively discriminated against gamma radiation, because electrons produced by a gamma ray could deposit very little energy in the sensitive layer. Thus, gamma-ray induced pulses were all very small compared to the majority of pulses from neutron captures. This was observed by means of a pulse-height analyzer, and the discriminator bias of the main amplifier was set to eliminate all possible gamma-ray counts.

The cross section for the reaction $B^{10}(n, \alpha)Li^{7}$ is known to follow the 1/v law quite accurately from thermal energies to about 500 keV (Hughes and Schwartz, 1958). Threshold neutrons from $Li^{6}(p, n)Be^{6}$ have an average energy of 123 keV in the laboratory (see Part III), so that their detection probability is a factor of 2000 smaller than that for thermal neutrons. To improve the counting rate with respect to background, a poly-

ethylene moderator was inserted in front of the detector. For optimum performance, the size of the moderator should be chosen large enough to give an appreciable probability for thermalizing threshold neutrons, but small enough so that few of the higher energy background neutrons will be thermalized.

A moderator 2.62 cm thick was used for the thereshold measurements, corresponding to about five mean free paths for thermal neutrons. From a larger diameter of 5 cm, matching that of the detector, it was tapered to a 14° truncated cone, reducing somewhat the moderation path for neutrons generated in the beam-defining aperture ahead of the target.

This aperture was located 25.7 cm from the target, and consisted of 0.05 cm gold sheet, about 2 cm square, with a 0.25 cm hole on the beam axis. Since the background from the aperture was critically dependent on the shape of the beam, it was necessary to measure it in direct sequence with each run on the target, without changing the beam focus.

3. Long Counter

A long counter of standard design (Hanson and McKibben, 1947) was located 28.3 cm from the target at 90° to the beam during the measurements. It served as a monitor and check on the changes in counting rate observed with the threshold detector, but was found to be much more susceptible to errors in background subtraction due to changes in beam focus. Thus, it could not be used in the detailed study of the threshold behavior. Since it is designed to have nearly constant efficiency for neutrons from 0.1 to over 10 MeV, the long counter does indicate the general charac-

teristics of the reaction cross section, and the data from it will be presented in this sense.

Pulses from the $B^{10}F_3$ proportional counter tube (RCL Model 10512) of the long counter were amplified and stored by apparatus identical to that used in conjunction with the threshold counter. The discriminator level was independently set to include all pulses in the rather broad spectrum produced in the tube by neutron capture reactions in the B^{10}. The sensitivity to gamma rays was found to be small; no appreciable difference between the spectra from a Ra-Be neutron source and those from the various neutron-producing reactions could be observed.

There seemed to be no appreciable effect due to the scattering of neutrons from the long counter into the threshold counter or vice versa. The counting rates remained the same within statistics when one or the other was removed. A cadmium shield around the threshold detector system captured thermal neutrons which might have passed between the two counters. The solid angle subtended by the long counter was 0.4 steradian.

4. Beam-handling Equipment

The energy of the incident beam was determined by the 90° magnetic analyzer. The analyzer is of the homogeneous-field type, focusing the beam only in the radial direction. The radius of the particle orbits in the magnet is 86.3 cm. The entrance and exit slits were adjusted to a width of 0.508 cm for the runs measuring the neutron production on a large scale over the entire energy range. For the detailed measurements of the shape of the Be^6 ground-state threshold, the slits were set to a width of 0.102 cm.

The corresponding homogeneity of the beam energy, $\delta E/E = 2\delta R/R$, was 12 parts per thousand in the former case, 2.4 parts per thousand in the latter.

The magnetic field of the analyzer was measured by a nuclear magnetic resonance fluxmeter. The frequency f of the proton magnetic resonance, determined from a probe located in the analyzer gap near the beam path, is related to the energy E of the particles passing through the analyzer by the formula:

$$E\left(1 + \frac{E}{2Mc^2}\right) = k\,\frac{Z^2}{M}\,f^2 \quad ,$$

correct to relativistic first order. Z and M are the charge and mass of the ions in the beam. The constant k was determined by measuring sharp neutron thresholds with well-known threshold energies. Because of possible nonlinearities in the magnet, the most desirable calibration reaction should have a threshold energy near the one to be measured. The $Al^{27}(p, n)Si^{27}$ reaction with a threshold energy of 5.797 ± 0.004 MeV (a weighted average of the values given by Bromley, et al., (1959)) was the best from this point of view. The energy scale for the most accurate Be^6 threshold run was based on an immediately subsequent run with a superpure aluminum target. This calibration point could be determined within 3 keV by plotting the 2/3 power of the counts vs. frequency (Bonner, 1960; Marion, 1961).

Focusing of the beam onto the target was accomplished mainly with a magnetic quadrupole lens, located 5.2 m beyond the exit slit of the analyzer, and 6.5 m in front of the target. The position of the beam was adjustable by the use of two small steering magnets located near the quadrupole. The beam spot could be observed by means of a piece of quartz mounted on the target holder. The other focusing devices of the accelerator were found to have a much smaller effect on the size and shape of the beam at the target position.

The charge of the particles constituting the bombardment for each point was determined by an Eldorado Model CI-110 current integrator. The loss of secondary electrons from the target was restricted by its battery bias of +300 V. relative to a tube of tantalum foil at ground potential in the entrance neck of the target chamber. A charge of 50 microcoulombs was used for most of the measurements. Although the integrator was checked periodically and found to be accurate to $\sim$ 3% of the scale reading, an absolute charge measurement was not used in obtaining the results. All of the threshold measurements depend only on the charge collected being constant for each point throughout the run. Checks of the stability of the integrator made before and after each run showed a deviation of less than 0.3% in the charge measurement.

III. DETECTOR RESPONSE AT THRESHOLD

1. Introduction

In order to determine the threshold energy and the width of a level such as the Be^6 ground state, it is necessary to interpret the data obtained over a range of beam energy comparable to or larger than the width to be measured. Thus, it is insufficient to rely simply on the fact that the response for a zero-width final state must be characterized by a discontinuous rise as the bombarding energy increases above threshold. One must know the detailed shape of the response above such a sharp threshold for an energy range of a few times the expected width. The threshold curve for the wide final state is actually a convolution of a function depending on the nuclear properties of the reaction (cross section and final state characteristics, which will be discussed in the next chapter), with an experimental factor depending on the detector response and the incident energy variation due to the beam spread and stopping in the target layer.

The response function of the detector in itself reflects the combined effects of a number of physical processes. These have to do with the kinematics of the particular reaction being observed at threshold, the degradation of the spectrum of neutron energies due to the moderator, and the energy dependence of the counting efficiency in the detector.

2. Threshold Kinematics

First, a brief discussion of the kinematics at threshold We consider final states of definite mass, appropriate to the response function desired. At the exact threshold, neutrons appear only at 0^{o} with energy E_{n0} corresponding to the center of mass velocity v_{cm}. Above threshold, the neutrons leave the reaction with a small velocity in the center of mass system. Added vectorially to the laboratory velocity of the center of mas itself, the neutron velocities correspond to a range of energies roughly centered on the initial threshold energy E_{n0}, and all neutrons appear within a cone about the forward direction in the laboratory.

It is useful to discuss the kinematics in terms of the quantity $\epsilon = E_1 - E_{th}$, which is the energy of the bombarding particle in excess of the threshold energy. The angle of the neutron cone increases with ϵ. The neutrons which are to be detected must have their direction within the cone of the solid angle subtended by the counter system. Below a certain value of ϵ, designated ϵ_{α}, all of the neutrons from the reaction arc within this cone and must enter the moderator. When $\epsilon > \epsilon_{\alpha}$, some of the neutrons do not intercept the detecting system, and this fraction of lost neutrons increases as ϵ becomes larger. At a certain value which may be designated ϵ_{π}, the limiting angle of the neutron cone opens to 180^{o}, and above this point the neutrons may be emitted in all directions in the laboratory system. These conditions are shown graphically in Figure 3.

At threshold, where $\epsilon = 0$, neutrons entering the moderator are monoenergetic, with energy $E_{n0} = 1/2\ m_n v_{cm}^2$. One can estimate the relative efficiency for detecting these neutrons after moderation; for the 123 keV neutrons appearing at the Be^6 threshold, the moderator is about three mean free paths thick. In passing through the moderator, the neutrons acquire an energy distribution which is spread between zero and the upper limit E_{n0}. The shape of this spectrum depends on the average number of collisions made by a neutron on its way through the moderator. An estimate for the efficiency would result from weighting this spectrum by the 1/v capture probability in the detector, normalizing to the 35% efficiency for thermal neutrons quoted by the manufacturer, and integrating.

For $\epsilon > 0$ such a simple approach is not adequate, because of the complicated behavior of the neutron spectrum passing into the moderator. Just above threshold there is a range of energies approximately centered on E_{n0}. For $\epsilon_\alpha < \epsilon < \epsilon_\pi$, one finds two bands of neutron energies entering the moderator. The lower energy band contains fewer neutrons if the angular distribution is isotropic in the center of mass system, as can be seen from Figure 3. Above ϵ_π, the low energy neutrons have reversed direction, and only the faster neutrons may be counted. Because

of the 1/v counting probability, this implies that the counting rate should decrease more rapidly as the value of ϵ increases above ϵ_π.

3. Response Calculations

The relative efficiency was calculated for several values of ϵ using a Monte Carlo program on the Cal Tech IBM 7094 computer. The results are shown in Figures 4 and 5. A description of the response function program can be found in Appendix A.

The Monte Carlo threshold calculation yields points for $F(\epsilon)$ which approach the required response function as the number of neutron paths in the calculation is increased. In order to keep the computer time used down to a reasonable value, the calculations were cut off when the fluctuations in the value of F became relatively small. The remaining statistical differences from the values which would result from the impractical calculation of an infinite number of neutron paths is apparent from Figure 4, since the points do not define a smooth curve. For the purposes of the data analysis integrals, it is necessary to have $F(\epsilon)$ for a large number of intervals of ϵ. An analytic approximation to the smooth response which the Monte Carlo points approach is expedient in this connection. The function shown in the figure is represented by two negative powers of ϵ, with a break at ϵ_b connecting the two parts of the function. It is easily obtained by drawing the two lines on the log-log plot which appear to agree best with the calculated points. Extrapolated to the left, it gives $F(0) = \infty$, which cannot be true of the actual response

function, but the integrals in Part IV only make use of the function for $\epsilon > 5$ keV.

S-wave neutrons must be distributed isotropically in the center-of-mass system, and the Monte Carlo response calculation used this distribution. However, in the case of both incoming and outgoing p-waves, an anisotropic angular distribution is possible, which would distort the threshold response. A calculation of the possible anisotropy was made by assuming that the reaction proceeds through a $3/2^-$ state in Be^7. The result is a distribution proportional to $1.05 - 0.15 \cos^2\theta$, which is probably close enough to being isotropic to justify using the same $F(\epsilon)$ for both s- and p-waves.

Since the calculation of the response function from the properties of the detector system is rather involved, an empirical check of the result is desirable. Appendix B describes such a check made by measuring a sharp threshold with the system. Unfortunately the function cannot be verified exactly because of the unknown relative intensity of s- and p-wave neutrons. However, the test does indicate the possible range of error of the calculated function with respect to the actual response of the system.

The eventual disposition of neutrons as a function of ϵ is shown in Figure 5. The percentages of all neutrons produced in the reaction are calculated as a part of the Monte Carlo threshold program. The kinematics of the Be^6 threshold were used for the results in this figure. The relative losses for various ϵ may be useful as a guide for the design of an improved moderator-detector assembly. It is apparent that the design must depend on the particular reaction to be studied.

IV. ANALYSIS OF THE DATA AT THRESHOLD

1. Background

Measurement and subtraction from the data were done separately for each of the two major sources of background. Reactions in the gold target backing and beam collimator constituted one source; reactions with the Li^7 impurity in the enriched Li^6 target material were responsible for the other.

Neutrons from the gold target blank and beam-defining aperture were counted immediately preceding or following each run on the lithium target, using the same charge integration. The beam current and focus were not changed between the two runs, so that the fraction of beam striking the aperture would remain as nearly constant as possible. The difference in counts between the runs at each energy is presumed to be due to reactions in the lithium layer only. The resulting points are plotted in Figure 6.

Any drift in the beam position relative to the aperture is certainly a source of systematic error. The first run of each pair was alternated between the lithium target and the clean backing. This would cause the systematic errors in the sequence of points to have alternately opposite signs after subtraction, provided that the beam drift did not change over a time interval corresponding to several integrations. Of course, changes with a period much shorter than an integration would average to zero error after subtraction. Thus, the general shape of the curves should be correct, with distortions from this source only in the

unlikely case of the beam changing its direction of drift on the order of once in each integration.

Below 4 MeV, the background from the gold was negligible, so that blank-target runs for each point were unnecessary. Its increase above 4 MeV was approximately exponential with bombarding energy.

The data below the region of the Be^6 threshold exhibit the characteristics of the Li^7(p, n)Be^7 excitation function, namely the sharp threshold at 1.8807 MeV and resonances at 2.3 and 5 MeV corresponding to excited states in Be^8. The Li^7 occurs as an impurity in the enriched Li^6 used to make the targets. To determine the background from this source above 5.5 MeV, a natural lithium target was made in place of the Li^6 target, and measurements made through the same range of energy. At the higher energies, the gold background was subtracted as described above. The Li^7(p, n)Be^7 cross section is much larger than that for the Li^6(p, n)Be^6 reaction, and the threshold for the latter cannot be observed in this data, also shown in Figure 6, although natural lithium contains 7.5% Li^6. This also meant that the gold, which provides a background to the background determination here, was a less significant source of error than in the main Be^6 threshold runs. A higher threshold at 7.07 MeV can be seen which is due to the 4.54 MeV level in Be^7.

The data from the natural lithium target was normalized to that from the Li^6 target at the 2.3 and 5 MeV resonances. It was then converted into a smooth curve in the region 5.5 to 6.3 MeV so that it could be subtracted without intensifying the statistical fluctuations. The resulting points are given in Figure 7.

2. Stopping in Target and Spread of Beam Energy

The presence of the Li^7 impurity was not entirely a disadvantage. It allowed the target thickness be estimated by finding the detailed shape of the curve near the Be^7 threshold at 1.8807 MeV. Since the energy loss in the target was small compared to the width to be measured at 5.9 MeV, an upper limit to the thickness was sufficient. If the incident protons lose an amount of energy ΔE in passing through the target layer, the counting rate must rise monotonically between $E_p = E_{th}$, where reactions can only occur at the front surface of the target, and $E_p = E_{th} + \Delta E$, where reactions may occur throughout the target volume. A maximum in the counting rate may occur at some slightly higher energy E_{max}, due to a changing cross section and the threshold response of the detector system discussed in the previous chapter. Thus, we can measure $E_{max} - E_{th} > \Delta E$, which gives the required upper limit.

Data from the target used for the width measurement are shown in Figure 8. The observed value of $E_{max} - E_{th} = 25$ KeV. The Lindhard-Scharff law for stopping powers, which has been verified by McCray (1962, 1963) up to 3 MeV for lithium, was used as given in the graphs of Whaling (1958). At 5.9 MeV beam energy, the proton energy loss in the target is calculated to be $\Delta E < 12$ keV.

The spread in beam energy and stopping loss in the target layer may be combined in analyzing the data. An effective spectrum of protons incident on target nuclei is used, which is a convolution of a rectangular penetration distribution due to the assumed uniform target layer with the shape of the beam energy

distribution. The latter is usually assumed to be triangular, which would be the result of a spatially uniform beam with a broad energy spread passing through the two slits of the analyzing magnet. The real beam has deviations from both of these properties: it is brought to a focus near the exit slit by a magnetic quadripole lens, and the accelerator is regulated to provide a distribution in energy peaked at the value being accepted by the analyzer. Both of these properties tend to produce an analyzed beam distribution which is more sharply peaked than a triangle. In the absence of a measurement of this distribution, which may well vary from time to time as the machine controls are adjusted, it was considered to be triangular, with a base width corresponding to the sum of the slit settings. This width was about 28.8 keV in the vicinity of the Be^6 threshold. The resulting rectangle-triangle convolution ξ (E) used in the fitting integral was $\sim$ 18 keV wide at half maximum.

3. Data Fitting

Calculated threshold curves were fitted to the data points to find the best values for the parameters which could be determined for the reaction. Two of the parameters used to obtain the calculated curves were in the form most directly related to the data, namely the threshold energy E_{th} and the width Γ_0 of the Be^6 level formed. By comparing the curves for various values of the width, one sees that the characteristics sensitive to this parameter are the slope and curvature near threshold, particularly on the low-energy side. Different values of the threshold energy simply translate the entire curve along the energy axis. The change in shape of the curve for

various threshold energies is so slight as to be unnoticeable over a range including most of the rise of the curve. This is because the difference between the Be^6 threshold and the α + 2p threshold, where the neutron yield must vanish, is much larger than the threshold width.

The shape of the curve above its maximum depends mainly on the relative strengths of the neutron partial waves. S- and p-wave coefficients comprised the remaining fitting parameters.

Using the expression

$$S(E_p) = \sum_{\ell=0,1} C_\ell \int \xi(E_p - E)\, S'_\ell\, (E,\, E_{th},\, \Gamma_0)dE \quad , \qquad (1)$$

least-square fits to the data were made to determine C_0 and C_1. This was done for several pairs of $(E_{th},\, \Gamma_0)$ values and the fits compared by tabulating χ^2. A least-squares adjustment between adjacent pairs was also made to insure that the results would be consistent with a best fit. In the above expression, the beam energy E_p corresponds to the measured analyzer field for each data point. The integral extends over a range of E for which $\xi(E_p - E) \neq 0$, as determined by the beam spread and target thickness. The s- and p-wave contributions are given by

$$S'_\ell\, (E,\, E_{th},\, \Gamma_0) = B_\ell(E) \int_0^{E - E_0} F(\epsilon)\, P_\ell^{(n)}(\epsilon)\, \rho_6(E-\epsilon,\, E_{th}, \Gamma_0)d\epsilon. \quad (2)$$

The functions involved are described in the following paragraphs. E_0 = 4.32 MeV is the α + p + p + n threshold, below which no free neutrons can be produced.

$B_\ell(E)$ represents the resonance behavior of the compound nucleus. For $\ell = 1$, $Be^6(0^+) + n$ could be formed from a $1/2^-$ or $3/2^-$ level in Be^7. The first can be made by p-wave protons on $Li^6(1^+)$, the second by p- or f-wave protons. The nearest such level is at 9.9 MeV, which has been observed as a p-wave scattering resonance at 5.1 MeV proton energy by Harrison (1964).

The resonance parameters measured by Harrison (1964) were used to calculate the p-wave resonant factor:

$$B_1(E) = \frac{2.89\, P_1^{(p)}(E_c)}{2.163E_c^2 - 18.81E_c + 42.69} ,$$

where $E_c = 0.856\ E$ is the center-of-mass energy and $P_\ell^{(p)} = kR/(F_\ell^2 + G_\ell^2)$ is the proton penetration factor. The constant 2.89 was chosen to give $B_1/P_1^{(p)}$ unit value at the Be^6 threshold. A radius $R = 4.4$ fm was used.

In the case of $\ell = 0$, only a $1/2^+$ level in Be^7 formed by s- or d-wave protons can contribute to the production of $Be^6 + n$. There is no evidence for such a level in the vicinity of this threshold. For this reason, the s-wave factor was considered to be nonresonant:

$$B_0(E) = P_0^{(p)}(E_c) . \qquad (3)$$

$F(\epsilon)$ is the detector response calculated by the Monte Carlo threshold program, which is discussed in Part III and Appendix A.

For the purpose of folding $F(\epsilon)$ into the above integral, it was approximated by a two-part power law function, which is indicated graphically in Figure 4:

$$F(\epsilon) = \begin{cases} 0.841\ \epsilon^{-0.145} & \text{if} \quad \epsilon < 0.0675 \text{ McV} \\ 0.0566\ \epsilon^{-1.145} & \text{if} \quad \epsilon \geq 0.0675 \text{ MeV} . \end{cases} \tag{4}$$

The neutron penetration factors are given by:

$$P_0^{(n)}(\epsilon) = kR \ , \qquad P_1^{(n)}(\epsilon) = \frac{(kR)^3}{1 + (kR)^2} \ , \tag{5}$$

for s-wave and p-wave neutrons respectively. These are approximations valid when the momentum $\hbar k \propto \sqrt{\epsilon}$ of the neutron outside the nuclear region is much less than that inside the nucleus (Blatt and Weisskopf, 1952). This is certainly the case near threshold, where the factors are most important. Other constant factors, which do not depend on ℓ, are taken into the C_ℓ . An interaction radius of R = 4 fm was used here in order to be consistent with the radii occurring in the decay-mode calculations. It is also not far from the radius obtained from the (1.4 fm) x $A^{1/3}$ rule, although there is really no justification for using it with such light and loosely bound nuclei.

The coefficients C_0 and C_1 contain, besides a normalization constant which is the same for both, factors depending on the intermediate states of the s- and p-wave reactions. The reduced widths for s- and p-wave protons and neutrons occur multiplied by a statistical factor $2\ell + 1$. Since the B_ℓ factors are arbitrarily set equal to P_ℓ at the Be^6 threshold, other factors taken into the C_ℓ are related to the resonance energies of the Be^7 levels involved. Only the ratio $U = C_1/C_0$ can be determined from fitting the data in this experiment. Without more information about the separate quantities it is difficult to ascribe a meaning to the value of U obtained.

4. Density of Final States

The density of final states function ρ_6 in Equation (2) is similar to those described by Barker and Treacy (1962). Its shape as a function of energy is, except for a penetration factor, exactly the shape of the particle spectrum expected from any reaction in which Be^6 is the residual nucleus. In general, it has a resonance shape with some degree of distortion, which in certain cases gives a secondary peak known as a "ghost". In the case of Be^6, the shape of ρ_6 depends on whether a proton or an α particle is considered to be emitted first in the decay.

The density of final states was obtained from the expression:

$$\rho_6 = \frac{1/2\ \Gamma(E')}{\nu^2\ (E_{th} - E')^2 + 1/4\ \Gamma(E')^2}\ , \qquad (6)$$

where the energy variable in the laboratory system is $E' = E - \epsilon$, and the center-of-mass conversion factor $\nu = 0.856$.

The width function $\Gamma(E')$ described in Appendix C was approximated by the power law expression

$$\Gamma(E') = \Gamma_0 \left(\frac{E' - E_0}{E_{th} - E_0} \right)^{\mu} , \tag{7}$$

for the integration of (2). It has the value Γ_0 at the Be^6 threshold. In terms of the quantities in Appendix C, the threshold energy is given by

$$E_{th} = \nu^{-1}(E_B + \Delta_B) = -\nu^{-1}Q , \tag{8}$$

where $\Delta_B(E')$ is approximated by a constant. The power μ in Equation (7) was determined by the nature of the decay mode being considered.

The diproton + α mode required the calculation of ρ_2, representing the density of states of the proton-proton interaction. The p - p scattering at the low energies in question is entirely s-wave, and can be described by the effective range theory. The phase shift δ was calculated from (Moravcsik, 1960):

$$C^2 \cot \delta + 2\pi\eta h(\eta) = -\frac{1}{ka} + 1/2\, kr_0 - Pk^3 r_0^3$$

$$\eta = \frac{e^2 M_p}{2\hbar^2 k} \quad ; \quad C^2 = \frac{2\pi\eta}{e^{2\pi\eta} - 1} \tag{9}$$

$$h(\eta) = -0.57721 \ldots \; -\ln\eta + \eta^2 \sum_{n=1}^{\infty} \frac{1}{n(n^2 + \eta^2)} \quad ,$$

where the scattering length a = -7.77 fm, the effective range r_0 = 2.77 fm, and the shape parameter P = 0.047. This phase shift was used in the formulae in Appendix C, with the penetration factor and hard sphere phase shift calculated using an interaction radius of 2 fm. Figure 9 shows ρ_2 and the corresponding ρ_6. The value of μ in the power law approximation of Γ decreased steadily from more than 6 at the α + 2p threshold. In a range of about one MeV around the Be^6 ground state, μ = 3.32 gave a reasonably good agreement, so this value was used in Equation (7) for the diproton + α mode.

In the calculation for the Li^5 + p decay mode, the secondary density of states, ρ_5, representing the $Li^5 \rightarrow \alpha$ + p decay, was obtained by the methods described in Appendix C. The parameters used were those calculated (Tombrello and Bacher, 1964) from measurements of α + p scattering (Miller and Phillips, 1958):

$$\gamma_5^2 = 7.0 \quad \text{MeV}$$

$$E_5 = 4.16 \quad \text{MeV} \qquad (10)$$

$$R_5 = 3.0 \text{ fm} \; .$$

ρ_5 and the density ρ_6 derived from it are shown in Figure 10. The power law approximation for $\Gamma(E)$ in (7) had the value $\mu = 6.61$ in the vicinity of the Be^6 ground state. The approximation is good from the α + 2p threshold to about one MeV above the ground state.

For both of the above cases, the penetration factors for the initial decay of Be^6 were calculated using an interaction radius of 3.5 fm.

An additional set of fits was made with $\mu = 0$. This represents a constant $\Gamma(E') = \Gamma_0$ which means that the penetration factors of the decay products are independent of energy. This is not a realistic assumption, but can be considered as one limiting case of three-body breakup in which the forces between the final particles are small and the radius of interaction is large. K is distributed between zero and a maximum for each particle, but if R is large enough, the penetration factor could be nearly constant. This may be consistent with the average potential of three unbound particles. This case is designated "symmetric" because the Breit-Wigner resonance shape is not distorted by final state interactions.

Figure 11 displays the results for E_{th} and Γ_0 obtained from fits in these three modes. The contours represent values giving an equally good fit, as measured by χ^2. One can see that Γ_0 is the more sensitive to the differences between modes.

The distortion of ρ_6 in either of the sequential decay modes produces a very low $S(E_p)$ in the region more than 150 keV below the threshold energy. It is clear from Figure 7a that the level of the data points in this region, although relatively low compared

with points above threshold, is too large to be fit with any combination of parameters for all but the symmetric case. The counting rate for these points is small compared with that of the background. The main background error is expected to arise from the normalization of the Li^7 measurements. Since the background was approximated by a smooth curve before subtraction, this error is systematic and does not affect the shape of the threshold. Thus, it may be represented as a possible shift of the base line. The standard deviation of the base line for the data shown in Figure 7, estimated from the normalization of the Li^7 background at the 2.3 MeV resonance, is 160 counts. An additional, unknown error in the base line is that due to possible target impurities (C^{13}, N^{15}, O^{18}) for which (p, n) reactions occur at this energy.

To determine the effect of these errors, calculations were made with the base line adjusted to give a good fit to the lowest ten points. The result for an adjustment of 202 counts for the diproton + α case is shown in Figure 7b, and a similar fit was obtained for the Li^5 + p case with an adjustment of 307 counts. Figure 12 shows the values obtained from these fits, Γ_0 being most significantly affected by this adjustment. This sensitivity to small systematic background errors below threshold seems to be an unavoidable characteristic of the method.

Another factor which could influence the results is the deviation of the function $F(\epsilon)$ used in the fit from the true counter response. To test the sensitivity to such a deviation, $F(\epsilon)$ was replaced by similar functions with different break positions ϵ_b. At the upper end, $\epsilon_b = \epsilon_\alpha = 123$ keV was chosen as an extreme limit,

corresponding to a drop in counting rate due only to the neutron cone opening wider than the detector cone. Losses from the front and side of the moderator are ignored, so this may be considered as the equivalent to surrounding the moderator with a neutron reflector. At the lower end, ϵ_b = 30 keV was chosen. The corresponding results are indicated by the limit marks in Figures 11 and 12. The $F(\epsilon)$ test described in Appendix B suggests that smaller limits would be appropriate for calculating the overall errors. Using the relative limits found there, the break for this $F(\epsilon)$ should lie on the range 40 keV $< \epsilon_b <$ 80 keV, the value obtained from the plot of the Monte Carlo points being 67 keV.

V. INTERPRETATION OF THE MEASUREMENTS ABOVE THRESHOLD

1. Data from the Threshold Detector

Counts which can be attributed to neutrons from the reaction of Li^6 with protons were observed well above the Be^6 threshold. Figure 6 exhibits a curve rising with little apparent structure from 6.4 to 10.5 MeV, corresponding to about 4 MeV of excitation energy in Be^6. At the higher energies along the curve, statistical scatter of the points, caused by the high yield from the gold backing, tends to obscure any details which may be present. Neutrons from the Li^7 reaction contribute less than a tenth of the counting rate in this region and have no observable influence on the shape of the curve.

The fact that the curve begins to rise about 400 keV above threshold is evidence that the Be^6 ground state is not the only intermediate nuclear state involved in the reaction. Although the response function is not definitely known for the higher energy neutrons leading to that state at the bombarding energies considered here, it is most probable that the counting rate corresponding to the ground state neutron group is either decreasing or leveling off as the proton energy increases. A strong resonance above 10 MeV might also produce this rise, but this hypothesis is refuted by the failure to observe such an effect in proton scattering experiments (Harrison and Whitehead, 1963). If the rise were due to a strong forward peaking of the ground-state neutron angular distribution, the long counter at 90^o would show a corresponding

decrease. This is contrary to the observations described in the next section.

Ajzenberg-Selove et al., (1959) have reported a neutron group from the same reaction corresponding to a narrow level ($\Gamma < 100$ keV) in Be^6 at about 1.5 MeV excitation. The only threshold feature which appears at the corresponding energy is the broad rise from 0.5 to 2 MeV excitation. If this is actually due to a state about 1.5 MeV wide, which would be the analog of the 1.71 MeV state in He^6, the width definitely disagrees with that of the neutron group reported. A possible explanation is given at the end of the next section.

2. Data from the Long Counter

The variation of sensitivity of the threshold detector system to neutrons of different energies means that the data obtained from it far above threshold is not simply related to the behavior of the reaction. The long counter, on the other hand, has a constant efficiency for neutrons of energies between 100 keV and over 10 MeV, so that it gives an indication of the variation of the cross section in the region above threshold. Since the sensitivity was low, giving poor statistics, and the background fluctuations were enhanced, only the gross structure of the long counter data can be considered significant.

The backgrounds from the gold and the Li^7 were subtracted in exactly the same manner as for the threshold detector data. Figure 13 shows the long counter data after subtraction of the gold background. Since the $Li^7(p, n)Be^7$ differential cross section has

been measured (Bevington et al., 1961), it could be used to establish the cross section values by determining the proportion of Li^7 to Li^6 in the target material.

Specifications from Oak Ridge National Laboratory, supplier of the enriched Li^6 metal, quoted 0.7% impurity of Li^7. A check on this value was carried out using a semiconductor surface barrier detector to measure the relative yields of charged particle reactions from targets made of the enriched Li^6. The proton and alpha particle groups from the Li^6 + p elastic scattering and the $Li^7(p, \alpha)He^4$ reaction were measured simultaneously. These cross sections have been fairly well established (McCray, 1962, 1963; Freeman et al., 1958). The results yielded the relation

$$\text{Atomic ratio } \frac{Li^7}{Li^6} = \frac{\alpha \text{ counts}}{p \text{ counts}} \times \frac{\sigma_6}{\sigma_7} = (1.0 \pm 0.2)\% ,$$

where the subscripts 6 and 7 refer to the scattering and (p, α) reaction respectively.

The long counter data was normalized using this value and the differential cross section at 90^o of the $Li^7(p, n)Be^7$ reaction between 3.3 and 4.0 MeV, which is in a nonresonant region, and seems to be a nearly constant 20 millibarns per steradian. The results for the $Li^6(p, n)Be^6$ differential cross section at 90^o are shown in Figure 14.

The differential cross sections reported by other experimenters are much smaller than the value obtained using the long counter measurements at the same energies. An example is

shown in Figure 14. At 10.5 MeV, the long counter registers about seven times as many neutrons as have been attributed to the Be^6 ground state neutron group.

The difference must be due to the fact that the above values from spectroscopy measurements give the cross section for producing the Be^6 ground state, while the long counter measures all neutrons produced from Li^6 + p at a given energy. These could include neutrons of lower energy than the ground state group. The tail of the ρ_6 density of states function is inadequate to account for this large difference, so there seems to be evidence for the occurrence of other processes. The possibilities include:

(1) Reactions leading to excited states in Be^6. The threshold detector results indicate that these would have to be very broad.

(2) Other reactions leading to neutron emission from secondary decays. One possible set is

$$Li^6(p,\ p')Li^{6*}(p)He^5(n)He^4 \ ,$$

$$\text{or} \quad Li^{6*}(n)Li^5(p)He^4 \ ,$$

$$\text{or} \quad Li^{6*}(\alpha)H^{2*}(n)H^1 \ .$$

One can also formulate sequences involving unbound states in He^3. If the time between successive decays is short enough, these processes could be termed "four-body decay".

(3) There may be multiple reactions of the type $Li^6(p, d)Li^5$; $Li^6(d, n)Be^7$ where deuterons from the first reaction interact with a second target nucleus.

The long counter data gives no information about the nature or relative significance of these processes. But it does indicate that they are collectively at least four times more probable than the $Li^6(p, n)Be^6$ ground state reaction at 9 MeV, when probable errors are taken into consideration.

An explanation for the sharp neutron group observed by Ajzenberg-Selove et al., (1959) may lie in considerations (2) or (3) above. Neutrons from a secondary decay may be limited to a relatively narrow group by kinematics. The threshold shape for the entire reaction sequence, however, is determined by the nature of the first particle emission. If the sequence begins with emission of a charged particle, the Coulomb barrier prevents any sharp increase in cross section at threshold. A typical exponentially increasing threshold curve results (Blatt and Weisskopf, 1952). This situation may account for the apparent contradiction between the two experimental observations.

For comparison with the results from the long counter data near threshold, the integral (IV. 2) was evaluated with the response function $F(\epsilon)$ replaced by a constant. This corresponds to using not only the flat efficiency characteristic of the long counter, but also ignores the kinematic solid-angle effects of the opening neutron cone. Thus, this calculated curve should actually be compared with data from a detector subtending 4π steradians of solid angle and having a constant efficiency for all energies. The 90^o position of the long counter made it rather insensitive to the

cone effects, so a comparison with this calculation should not have very great discrepancies if it is made somewhat above the threshold energy, at least by an amount equal to ϵ_{π} = 172 keV.

The parameters found in the fitting procedure for the diproton + α mode of decay were used in this calculation. The resulting curve is shown in Figures 14 and 15.

The excitation function has been measured recently (Bair et al., 1964) with a 4π solid angle detector. The data exhibit a smoothly rising curve above threshold in agreement with the present results. The estimated total cross section of 32 mb at 8 MeV is also consistent with the approximate differential cross section obtained from the above procedure.

VI. CONCLUSIONS

Three parameters were determined by the fitting procedure to the experimental threshold points. The value obtained for each parameter depended on the form used for the density of states function. Since the fits were about equally good in each case, they do not indicate which mode of decay is predominant, or which set of parameters is the correct one. It is necessary either to compare the results with other independent measurements, e. g., the spectroscopy experiments, or to make some physical arguments for preferring one mode over another.

The value obtained for the width is fairly sensitive to the different modes of decay, whereas the threshold energy is less so. The correlation between these values is indicated in Figures 11 and 12 by the elongated error contours. The fact that these are not aligned with the axes implies that these parameters are not independently determined from the data.

The results of the fitting procedure were values for E_{th} (or Q), Γ_0, and U which agreed best with the data. The first two were chosen at the centroid of the error contours. The set of values for these three parameters is sensitive to the mode of decay of the Be^6 ground state, as expressed in the form of the density of states function used in each fit. It is also sensitive to the error in subtraction of the Li^7(p, n)Be^7 background, which is most significant for the points somewhat below threshold, 5.6 MeV $< E_p <$ 5.8 MeV. If the decay proceeds predominantly by either of the sequential modes, (diproton + α or Li^5 + p), these points cannot be fit well. This strongly suggests that the background

has been underestimated. Increasing the assumed background by 1.3 standard deviations for the diproton + α case, or 1.9 standard deviations for the Li^5 + p case gives a more satisfactory fit. There is very little difference between these two fits, so the experiment does not determine whether one of the modes predominates.

When these adjustments are made, the resulting values of Q and Γ_0 are remarkably close for the two cases, as is apparent from Figure 12. Averaging the values for the two sequential decay modes, the results are:

$$\begin{aligned} Q &= -5074 \pm 9 \text{ keV} \\ \Gamma_0 &= 95 \pm 16 \text{ keV} \end{aligned} \qquad (1)$$

Allowance for a 50% error in the background adjustment increases the uncertainty in Q to ± 13 keV and that in Γ_0 to ± 28 keV.

Further considerations may be made, however, in selecting one of the modes as the more probable one, and thus narrowing the error limits. One possibility is to compare the results with those from the spectroscopy experiments. The neutron spectroscopy experiments have fairly large uncertainties in their reported values, and none of the widths agree very well with either of the values expected in this analysis. The results of Whaling (1964) from measurement of the $Li^6(He^3, t)Be^6$ reaction with a magnetic spectrometer, however, agree very well with the values expected for the diproton + α mode. A small correction in the values obtained directly from the spectra was made to allow comparison with the results of this experiment on Figure 12. This is due to the shape of ρ_6 which shifts the peak of the spectrum to a point corresponding to 3 keV below E_{th}, and gives a full width at half maximum which is 0.3 keV less than Γ_0. The shifts in the case of the Li^5 + p mode are 6 keV and 1.1 keV, respectively.

The error contour for this point overlaps the Li^5 + p contour to a slight extent, and the case for eliminating this mode is not very strong. It is, however, interesting to note the possibilities of using such a comparison in other reactions for determining the nature of decay mechanisms which cannot be observed directly.

It may be mentioned that the base line shift to obtain the best fit is smaller for the diproton + α mode than for Li^5 + p. Thus, the background corrections made on the basis of the Li^7 resonances are more compatible with the former mode, although again the latter is not excluded because of the systematic errors.

There remains the possibility of comparing the observed values for the width with those expected on the basis of general nuclear considerations. Let us express the total width as

$$\Gamma = \sum_i 2\bar{P}^{(i)} W_i \ \theta_i^2 \quad , \tag{2}$$

where $W_i = 3h^2/2\mu R^2$ is the Wigner limit for the ith decay mode, and θ_i^2 is of the order unity or less. $\bar{P}^{(i)}$ is the average penetration factor given in Appendix C. Putting in the values for Be^6 decay, we have

$$.095 = 0.238 \ \theta_{2,\,4}^2 + 0.00602 \ \theta_{5,\,1}^2 \ (\text{MeV}) \ . \tag{3}$$

Even if $\theta_{5,\,1}^2$ is near unity, the second term must be a small fraction of the total width, which means that the diproton + α mode represented by the first term must occur with much greater probability. A radius R = 3.5 fm was used in this estimate, but

any reasonable value of R will not change the above conclusion. For the second term to account for half of the total width, one would need R = 1.3 fm, which is even less than the p - p effective range.

The summation of transition probabilities (2) is consistent with the neglect of "true" three-body decay processes as described in Part I. It has been assumed that the time interval between sequential decays is long enough to distinguish, in principle, which particle was emitted first. Although such a measurement is far beyond the capability of present technique, it means that the probabilities must be added rather than amplitudes. Thus, there should be no interference between modes if the three-body amplitude is small.

The choice of the diproton + α mode of decay as the predominant one allows the use of the corresponding smaller error contour in Figure 12. The results on the basis of this choice, when the other experimental uncertainties are included, are the following:

$$\begin{aligned} E_{th} &= 5.924 \pm 0.011 \ \text{MeV} \\ Q &= -5.072 \pm 0.009 \ \text{MeV} \\ \Gamma_0 &= 0.085 \pm 0.011 \ \text{MeV} \ . \end{aligned} \qquad (4)$$

For completeness, the third parameter involved in this fit was the p-wave/s-wave ratio which took the value U = 20.3. A distinctly different value, U = 11.4, was obtained from the fit of the Li^5 + p mode. The error assigned to each value of U should probably be about 10%.

The only conclusion which can be drawn from the magnitude of U without supplementary information is that both even and odd parity states of the compound nucleus Be^7 contribute appreciably to the reaction near threshold.

The threshold measurement offers no conclusive evidence for an excited state in Be^6. If a state exists which is analogous to the 1.71 MeV state in He^6, one can say that it must be either very broad, or weakly produced in this reaction when compared with the ground state and the neutrons from secondary reactions described in Part V. The presumed spin of 2^+ may account for an inhibiting effect, since it could only be formed by $\ell \geq 2$ neutrons from the $1/2^+$ state in Be^7 which must be supplying the s-wave neutrons to the ground state if the latter has $J^\pi = 0^+$.

APPENDIX A. MONTE CARLO CALCULATION OF THE RESPONSE FUNCTION

The Monte Carlo method of determining energy and space distributions in a moderator or scattering medium has been applied to many neutron and gamma-ray problems (Cashwell and Everett, 1959). The basic technique is to calculate a multiply scattered path through the material for a large number of particles, using a random number, appropriately distributed, for each successive angle of scattering or path length between scattering centers. The neutron version of this established method was adapted in the present case to the kinematics of the neutron threshold.

The random number generator used is No. 1359 of the SHARE computer program library, and provides numbers randomly distributed on the interval between zero and one. Successive numbers r were produced from the formula

$$r_{i+1} = [nr_i + C] \qquad \text{(mod 1)}$$

where $n = 2^7 + 1 = 129$ and $C = 1/2 + \frac{\sqrt{3}}{6} = 0.78867\ldots$ are constants chosen to give the smallest correlation between successive values of r_i (Coveyou, 1960; Rotenberg, 1960).

Angular distributions, from the reaction itself as well as from all scatterings in the moderator, were assumed isotropic in the center-of-mass system, corresponding to s-wave neutrons. The first random quantity to be selected was the CM angle θ of the neutron emitted from the reaction, with respect to the beam direction. Isotropic distribution of this angle is equivalent to a

uniform distribution on the range $-1 < \cos\theta < +1$. Thus, it is necessary to set $\cos\theta = 2r - 1$. Since the moderator and detector have cylindrical symmetry about the beam direction, the azimuthal angle φ can be arbitrarily taken equal to zero. Next, the direction in the laboratory is calculated, and the procedure continues only if this lies within the cone subtended by the moderator.

The distance d, which is the path length in the moderator penetrated by the neutron before the first scattering, is exponentially distributed according to the usual rule. If λ is the mean free path of a neutron in the moderating material, the quantity $e^{-d/\lambda}$ is found uniformly distributed between zero and one. Thus, the next random number sets $d = -\lambda \ \ell n\, r$. The mean free path was found from the density of the moderator and the scattering cross section of the moderating nuclei (Hughes and Schwartz, 1958). Since the cross sections depend on the incident energy of the neutrons, the value of λ was selected from those given in Table I, according to the energy range occupied by the neutron after the last collision.

The nature of the scattering center was selected next on the assumption that the polyethylene moderator was composed of $(CH_2)_n$ molecules. The scattering would be from carbon if the relation

$$r > \frac{\sigma_H}{\sigma_H + 1/2\,\sigma_c} \quad ,$$

was satisfied, otherwise from hydrogen. The cross sections again were made to depend on which of the nine energy groups was occupied by the neutron.

The position of the scattering center was then compared with the boundaries of the moderator, and the calculation broken off if this was outside the polyethylene material. If the path crossed the detecting layer in back of the moderator, the neutron was considered counted with a weighting factor of $(v \cos \theta')^{-1}$, where θ' is the angle of the path with the normal to the plane of the detector.

If the scattering occurred inside the moderator, a new CM angle was chosen according to $\cos \theta = 2r-1$, and $\varphi = 2\pi r$. The procedure of finding path length, scatterer, and direction was repeated until the neutron could be considered either counted or lost by going outside the boundaries.

The scattering kinematics calculated in this way become invalid as the neutron energy approaches the thermal region, where the scattering centers have on the average as much kinetic energy as the neutrons. This is the region where the neutrons move by a diffusion process, neither gaining or losing energy as an ensemble. To account for this fact, another means of weighting was used for the group of neutrons which were slowed to thermal energy or lower. If the energy was found to be in this range after a collision, the neutron was treated as if it were a fluid diffusing uniformly throughout the moderator. The fraction of the moderator surface area facing the sensitive layer fixed the part of the "neutron fluid" which could be detected, and this fraction multiplied by the 1/v detection efficiency determined the weight to be stored as the effect of each thermalized neutron.

The form of the response function is simply the ratio of the total of weighted counts to the number of neutron paths calculated by the above method. A point results for each value of ϵ when the number of paths calculated is large enough to reduce statistical fluctuations to a small value.

The resulting function is proportional to the actual efficiency of the detection system. The constant of proportionality is difficult to determine, but it could probably be established empirically using a standard source such as $Li^7(p, n)Be^7$ with a calibrated target. This was not necessary for the present experiment, however, since the constant can be taken into the normalization factor discussed in Part IV.

APPENDIX B. VERIFICATION OF THE CALCULATED DETECTOR RESPONSE FUNCTION

1. Kinematical Reaction Parameters

The detector response function depends on the distribution in angle and energy of the neutrons incident on the detector system. This neutron dynamical distribution as a function of ϵ is determined by the two parameters E_{n0} and ϵ_{π}. The best verification reaction should therefore have these parameters as close as possible to those characterizing the $Li^6(p, n)Be^6$ threshold. Since a width factor should not be involved in the check, the reaction must produce only a neutron and a bound nuclear state. Table II gives the comparison of these parameters for the most favorable cases, as well as for the commonly used calibration thresholds, which are typical of the majority of neutron thresholds.

In addition to having kinematical characteristics in the proper region, the threshold to be used for an empirical test of the $F(\epsilon)$ calculation should be free from distortion by phenomena not relevant to the problem. In particular, strong resonances could produce a threshold shape quite unrelated to the value ϵ_b at which the response function falls off rapidly. The B^8 threshold was rejected for this reason: a strong resonance occurs very close to the threshold energy. The $Li^7(\alpha, n)B^{10}$ reaction exhibits only a weak resonance near $\epsilon = 0.3$ MeV, and was considered more suitable for the test.

2. Comparison of Results

Since the range of ϵ used in these runs is not a negligible fraction of the p-wave centripetal barrier, one expects to observe a combination of s- and p-wave neutrons. Their relative strengths depend on the neutron partial widths of states with opposite parity in the B^{11} compound nucleus. Since these are not known, the test of $F(\epsilon)$ is limited to showing that some combination of s- and p-waves can be combined with the response to give a curve which will agree with the measured threshold shape. Conversely, if the calculated $F(\epsilon)$ is assumed to be correct, the p-wave/s-wave ratio could be estimated. Higher ℓ -values were assumed to be unimportant.

The possible anisotropy of the p-wave neutron angular distribution in the center of mass system was not considered in making the comparison.

In Figure 16, the product $F(\epsilon)P_\ell^{(n)}(\epsilon)$ for s- and p-waves separately is compared with the measured $Li^7(\alpha, n)B^{10}$ threshold. The response $F(\epsilon)$ was calculated using the same Monte Carlo program as for the Be^6 threshold, changing only the appropriate kinematical constants to those for the B^{10} threshold. The p-wave penetration factor was approximated by $(kR)^3$, which is within 10% of the correct value for $\epsilon < 200$ keV. By normalizing the calculations to the data at $\epsilon = 100$ keV, where the break in the power law approximation of $F(\epsilon)$ occurs, it is seen that the measured points lie between the pure s-wave and pure p-wave limits. Since a linear combination of the two is expected, one may conclude that the calculated response is consistent with this data.

A more quantitative statement concerning the validity of the approximate response function can be made by considering the effect of shifting the value of ϵ_b. The range of $\epsilon_b = 100\ ^{+20}_{-40}$ keV satisfies the criterion that most of the measured points lie between the s- and p-wave limits. These uncertainties in ϵ_b were used to estimate the probable errors in the results of the Be^6 measurement due to deviation of the approximation from the true response function.

There is an additional source of error in this comparison due to the finite target thickness. When ϵ is less than the energy loss of α particles passing through the target layer, not all of the target nuclei can contribute to the yield. Thus, the points at small ϵ are depressed relative to the others. Also, for the purposes of this comparison, it would be more correct to plot the points at values of ϵ corresponding to the average α-particle energy in the target, rather than the beam energy. This change would again only be noticeable for small values of ϵ on the logarithmic scale. An improved plot would have the leftmost two or three points moved slightly up and to the left. As no additional target thickness measurement was made, these corrections are not indicated, but an estimate from the lithium evaporation gives no appreciable effect on the possible variation of ϵ_b described above.

APPENDIX C. CALCULATION OF THE DENSITY OF STATES FUNCTION FOR A SEQUENCE OF TWO-BODY DECAYS

The method for calculating the spectral shape of particles which leave a residual nucleus in an unstable state has been discussed by Barker and Treacy (1962). If the reaction to be considered is schematically defined as

$$A + a \rightarrow B + b\,;\ B \rightarrow C + c,$$

the spectrum of particles b is proportional to the density of final states

$$\rho_B(E) = \text{const}\ \frac{\Gamma_B(E)}{(E_B + \Delta_B - E)^2 + 1/4\ \Gamma_B^{\,2}}\ ,$$

where

$$\Gamma_B = 2P^{(c)}\gamma_B^{\,2} \qquad \Delta_B = -(S + \ell)\gamma_B^{\,2}$$

$$P^{(c)} = \frac{kR}{F^2 + G^2} \qquad S = kR\ \frac{FF' + GG'}{F^2 + G^2}$$

in terms of the Coulomb wave functions F and G at the radius R, and reduced widths γ^2. An alternate form is useful if the phase shifts are known:

$$\rho_B(E) = \text{const} \frac{\sin^2(\beta_c)}{P^{(c)}} \quad .$$

The resonant phase shift is given by $\beta = \delta + \varphi$, where φ is the hard sphere phase shift.

When the particle C can decay still further,

$$C \rightarrow D + d \quad ,$$

another density of states function involving the interaction of D with d enters the picture. This can be calculated by the same method,

$$\rho_C(E') = \text{const} \frac{\Gamma_C}{(E_C + \Delta_C - E')^2 + 1/4\Gamma_C^2} = \text{const} \frac{\sin^2(\beta_d)}{P^{(d)}} \quad ,$$

where E' is the energy in the rest system of C measured from the D + d threshold. The total decay energy of B may be partitioned many ways between c, d, and D, and a simple penetration factor $P^{(c)}(E)$ may no longer be used to get the energy dependence of Γ_B. The width must now be found by weighting all possible values of $P^{(c)}$ with the corresponding ρ_C and taking the mean:

$$\bar{P}^{(c)} = \frac{\int_0^E \rho_C(E')\ P^{(c)}(E - E')\, dE'}{\int_0^\infty \rho_C(E')\, dE'}$$

Then $$\Gamma_B(E) = 2\,\bar{P}^{(c)}\,\gamma_B^{\,2} \quad .$$

The level shift Δ_B must be calculated by a similar mean value formula. However, where the integral in the numerator above is cut off at the upper limit E by the vanishing of $P^{(c)}(E - E')$ for $E' \geq E$, this simplification does not occur for $S^{(c)}(E - E')$. In fact, the magnitude of S continually increases as $E - E'$ becomes more negative (Lane and Thomas, 1958). Thus, one must evaluate

$$\bar{\Delta}_B(E) = -\gamma_B^{\,2}\,\frac{\int_0^\infty \rho_C(E')\,S^{(c)}(E - E')\,dE'}{\int_0^\infty \rho_C(E')\,dE'} \quad ,$$

where the integrand in the numerator may be large in a region of $E' > E$, although to have a physically meaningful result the factor ρ_C must approach zero rapidly enough for large E' to make the integral converge. Since ρ_C is always positive, it is apparent that $\bar{\Delta}_B$ varies less rapidly with E than Γ_B. Furthermore, over a range of E corresponding to a smoothly varying ρ_C, $\bar{\Delta}_B$ may be considered to be constant to a good approximation.

REFERENCES

Ajzenberg-Selove, F., and Lauritsen, T., 1959, Nuclear Phys. 11, 1; 1962, Nuclear Data Sheets; 1965, Nuclear Phys., to be published.

Ajzenberg-Selove, F., Osgood, C. F., and Baker, C. P., 1959, Phys. Rev. 116, 1521.

Bair, J. K., Jones, C. M., and Willard, H. B., 1964, Nuclear Phys. 53, 209.

Barker, F. C., and Treacy, P. B., 1962, Nuclear Phys. 38, 33.

Bevington, P. R., Rolland, W. W., and Lewis, H. W., 1961, Phys. Rev. 121, 871.

Blatt, J. M., and Weisskopf, V. F., Theoretical Nuclear Physics (John Wiley and Sons, Inc., New York, 1952).

Bogdanov, G. F., Vlasov, N. A., Kalinin, S. P., Rybakov, B. V., and Sidorov, V. A., 1957, Soviet J. Atomic Energy 3, 987.

Bonner, T. W., in Nuclear Spectroscopy, Part A, F. Ajzenberg-Selove, ed., (Academic Press, New York, 1960).

Bromley, D. A., Ferguson, A. J., Gove, H. E., Kuehner, J. A., Litherland, A. E., Almqvist, E., and Batchelor, R., 1959, Canadian J. Phys. 37, 1514.

Cashwell, E. D., and Everett, C. J., A Practical Manual on the Monte Carlo Method for Random Walk Problems (Pergamon Press, New York, 1959).

Coveyou, R. R., 1960, J. Assoc. Computing Machinery 7, 72.

Freeman, J. M., Hanna, R. C., and Montague, J. H., 1958, Nuclear Phys. 5, 148.

Freeman, J. M., and West, D., 1962, Harwell Progress Reports, AERE-PR/NP 3 and 4.

Gulyamov, M., Rybakov, B. V., and Sidorov, V. A., 1963, Soviet Physics JETP 17, 1230.

Hanson, A. O., and McKibben, J. L., 1947, Phys. Rev. 72, 673.

Harrison, W. D., 1964, private communication.

Harrison, W. D., and Whitehead, A. B., 1963, Phys. Rev. 132, 2607.

Hughes, D. J., and Schwartz, R. B., 1958, Neutron Cross Sections, Brookhaven National Laboratory Report BNL 325.

Lane, A. M., and Thomas, R. G., 1958, Revs. Mod. Phys. 30, 257.

Marion, J. B., 1961, Revs. Mod. Phys. 33, 139.

Mattauch, J. H. E., Thiele, W., and Wapstra, A. H., 1964, Nuclear Phys., to be published.

McCray, J. A., 1962, thesis, Calif. Inst. of Tech., Phys. Rev. 130, 2034, 1963.

Miller, P. D., and Phillips, G. C., 1958, Phys. Rev. 112, 2043.

Moravcsik, M. J., 1960, Ann. Rev. Nucl. Sci., 10, 324.

Rotenberg, A., 1960, J. Assoc. Computing Machinery, 7, 75.

Tombrello, T. A., and Bacher, A. D., private communication.

Whaling, W., 1958, Handbuch der Physik, Bd. XXXIV p. 193.

Whaling, W., 1964, Bull. Am. Phys. Soc. 9, 627.

Table I. Group Parameters used in the Monte Carlo Threshold Calculation. The neutrons in each group have energies between the values given in the second column above and below the corresponding line. Mean free paths were calculated for polyethylene having a density of 0.917 g/cm^3. The last column gives the probability that the next collision is a hydrogen nucleus.

TABLE I. MONTE CARLO THRESHOLD MODERATOR COLLISION GROUP PARAMETERS

Group	Neutron Energy (lab.)	Mean Free Path (cm.)	H/C Probability Ratio
	0		
a.		(diffusion)	
	0.025 eV		
b.		0.5675	0.895
	5 keV		
c.		0.5941	0.891
	30		
d.		0.7174	0.872
	70		
e.		0.8553	0.850
	140		
f.		1.0916	0.818
	250		
g.		1.2838	0.799
	400		
h.		1.6056	0.785
	600		
i.		1.8932	0.776
	800		
j.		2.1609	0.767

Table II. Kinematical characteristics of some neutron thresholds. The quantities in the column headings are defined in Part III and Figure 3. The angle $\alpha = 58^{o}$ of the moderator cone used in the experiment was used for the values of ϵ_{α} given in the table.

TABLE II. KINEMATICAL CHARACTERISTICS OF SOME NEUTRON THRESHOLDS

Reaction	E_{n0} (keV)	ϵ_π (keV)	ϵ_α (keV)	E_{th} (MeV)
$Li^6(p, n)Be^6$	123	172	123	5.924
$Li^7(\alpha, n)B^{10}(0)$	145	266	188	4.39
$Li^7(\alpha, n')B^{10*}(.717)$	182	336	237	5.52
$Li^6(He^3, n)B^8$	110	198	140	2.97
$Li^7(p, n)Be^7(0)$	29.4	39	28	1.8807
$Al^{27}(p, n)Si^{27}$	7.4	8.0	5.7	5.797
$H^3(p, n)He^3$	64	128	89	1.019

Table III. Reduced data from the $Li^6(p,n)Be^6$ threshold. Counts given are the result of subtracting the gold and Li^7 backgrounds from the total recorded for each 50-μCoulomb bombardment with protons of energy E_p. The Li^7 background does not contribute to the statistical errors, because it was smoothed before subtraction. See pp. 21, 22 and Figure 7.

TABLE III. $Li^6(p, n)Be^6$ THRESHOLD DATA

Energy E_p	Counts S	Error ±	Energy E_p	Counts S	Error ±
5.587	167	86	5.956	6094	130
5.687	395	93	5.966	7214	134
5.697	456	94	5.976	7497	135
5.707	644	94	5.986	8061	137
5.717	611	94	5.996	8097	140
5.727	608	94	6.006	8655	143
5.737	571	95	6.016	9120	145
5.747	498	96	6.026	9629	147
5.757	797	96	6.036	9847	148
5.767	685	95	6.046	10084	149
5.777	485	93	6.056	10127	149
5.787	606	94	6.066	10214	150
5.796	551	94	6.076	10382	151
5.806	870	96	6.086	10455	152
5.816	718	97	6.096	10092	152
5.826	859	98	6.106	10074	152
5.836	829	98	6.116	10281	152
5.846	937	99	6.126	10047	152
5.856	1196	101	6.136	9952	151
5.866	1234	103	6.146	10073	152
5.876	1799	107	6.156	9697	151
5.886	2098	109	6.166	9598	151
5.896	2265	109	6.176	9334	151
5.906	2978	113	6.186	9513	151
5.916	3135	114	6.235	9361	153
5.926	4508	121	6.285	9220	156
5.936	5272	124	6.335	9727	161
5.946	5550	128			

Table IV. Sample results from the data-fitting calculations. Input parameters were used to calculate the curves which were fit to the data. A least-squares adjustment between fits for nearest input values gave the adjusted values shown. χ_{SD}^2 is the value of χ^2 which has a probability corresponding to one standard deviation from the minimum. The ratio U of the p-wave to s-wave coefficients is discussed in the text. See pp. 25, 28, 31, 32.

TABLE IV. SAMPLE RESULTS FROM DATA FITS

	Threshold Energy E_{th}(MeV)		Width Γ_0(keV)		P/S Ratio U	χ^2	χ_{SD}^2
	Input	Adjusted	Input	Adjusted			
μ = 0	5.900	5.908	40	56.6	103.4	360	286
(Symmetric)	5.900	5.909	45	57.1	103.6	290	
	5.910	5.920	50	62.6	58.9	284	
	5.910	5.921	55	62.7	58.5	260	
	5.910	5.921	60	65.0	58.2	286	
μ = 3.32	5.925	5.931	80	108.9	17.2	419	263
(diproton	5.925	5.931	90	109.4	16.4	282	
+ α)	5.925	5.931	100	109.5	15.7	243	
	5.930	5.929	100	105.1	13.4	238	
	5.930	5.929	110	103.8	13.0	241	
μ = 3.32	5.925	5.926	80	88.4	20.1	216	220
(diproton	5.925	5.926	85	87.9	19.7	200	
+ α,	5.925	5.926	90	89.3	19.3	207	
201.7 counts	5.930	5.931	85	97.5	15.6	258	
base adjust)	5.930	5.931	90	99.6	15.3	231	
μ = 6.61	5.925	5.932	100	107.4	13.7	200	189
(Li^5 + p,	5.925	5.933	105	107.1	13.6	215	
307.3 counts	5.930	5.933	100	108.4	11.5	175	
base adjust)	5.930	5.933	105	107.9	11.4	171	
	5.930	5.933	110	109.2	11.3	184	

Table V. Summary of the most significant probable errors in the determination of the threshold energy and width of the Be^6 ground state. The left-hand columns are based on the assumption that the diproton + α decay mode dominates, while the probable errors on the right include both this mode and the Li^5 + p mode. The net error given is the square root of the sum of the squares of the errors from all the sources. The sources of error are described on pp. 14, 31-33, 40-43, 51.

TABLE V. ERROR SUMMARY

	Errors in keV			
Decay Mode Assumed	diproton + α		both 2-body	
Quantity	E_{th}	Γ_0	E_{th}	Γ_0
Source of Error:				
1) Threshold fit	5	8	5	11
2) Detector response, Uncertain ϵ_b	8	6	8	6
3) Al^{27} calibration				
a) quoted E_{th}	4	-	4	-
b) measurement	3	-	3	-
4) Uncertain base line, Li^7 background and mode difference	2	4	10	25
Net error	11	11	15	28

Figure 1. Energy relations in the vicinity of the $Li^6(p,n)Be^6$ threshold. The possible states are shown in terms of the Be^7 compound nucleus and its partitions. Energy levels for Li^6, Be^7, and Be^6 in the relevant region are taken from Ajzenberg-Selove and Lauritsen (1962, 1965). The excitation energy in MeV is shown together with J^π were known. Cross-hatching indicates the approximate level widths for states near the Be^6 threshold. Numbers enclosed in rectangles are the mass differences in MeV from the Be^6 + n system. These are based on the value Q = -5.072 MeV obtained from the present experiment, with the remaining values calculated using the tables of Mattauch, Thiele, and Wapstra (1964). See pp. 1, 37, 38.

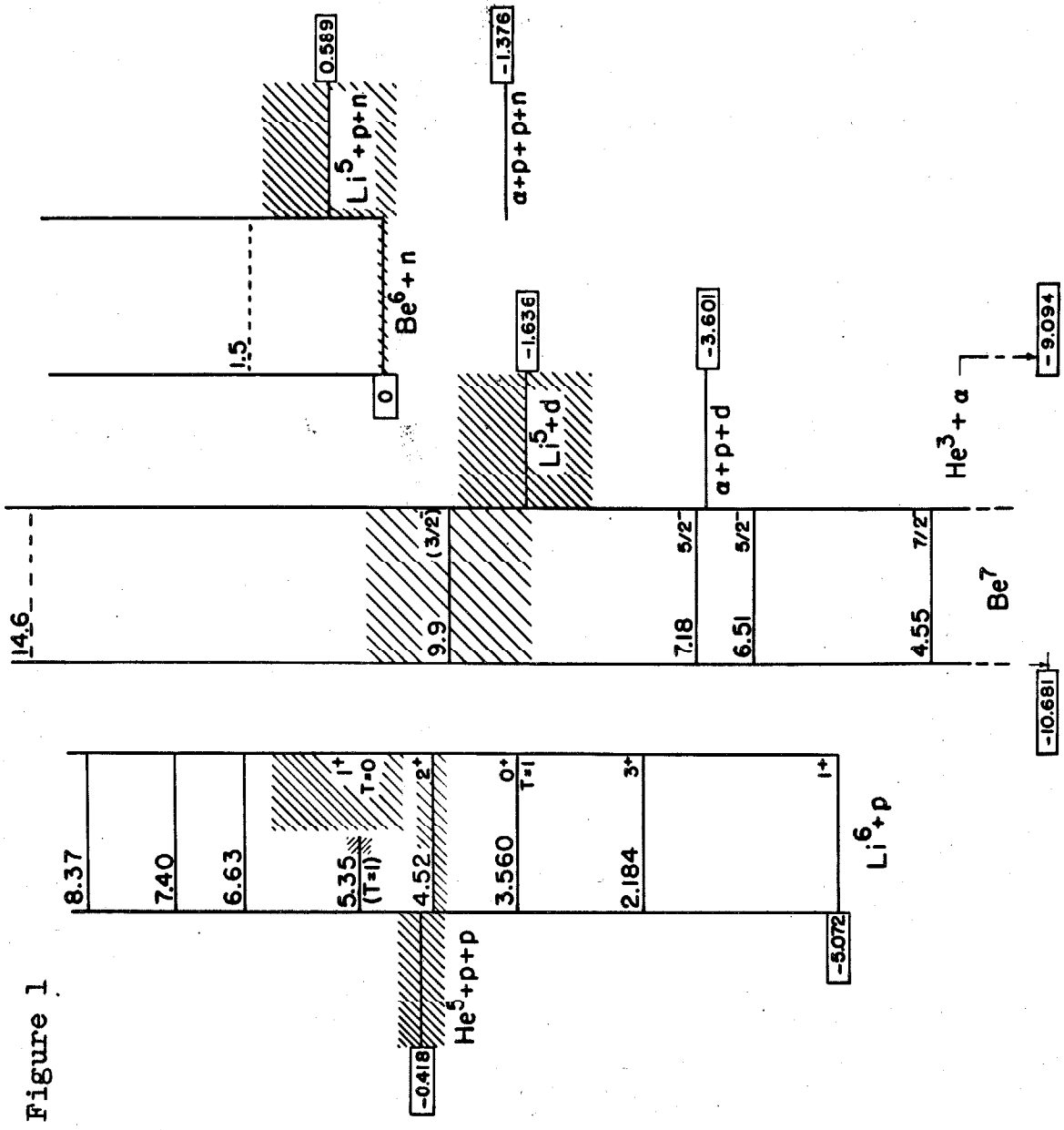
14.6
9.9
(3/2)⁻
7.18
5/2⁻
6.51
5/2⁻
4.55
7/2⁻
Be⁷
-10.681
He³+α
-9.094
α+p+d
-3.601
Li⁵+d
-1.636
α+p+p+n
-1.376
Be⁶+n
1.5
0
Li⁵+p+n
0.589
8.37
7.40
6.63
5.35
(T=1)
1⁺ T=0
4.52
2⁺
3.560
0⁺ T=1
2.184
3⁺
1⁺
Li⁶+p
-5.072
He⁵+p+p
-0.418

Figure 1

Figure 2. The experimental arrangement. The gold target blanks were mounted back-to-back on a rod perpendicular to the plane of the drawing and could be lowered into an adjacent chamber for evaporation of the lithium. See pp. 9-12.

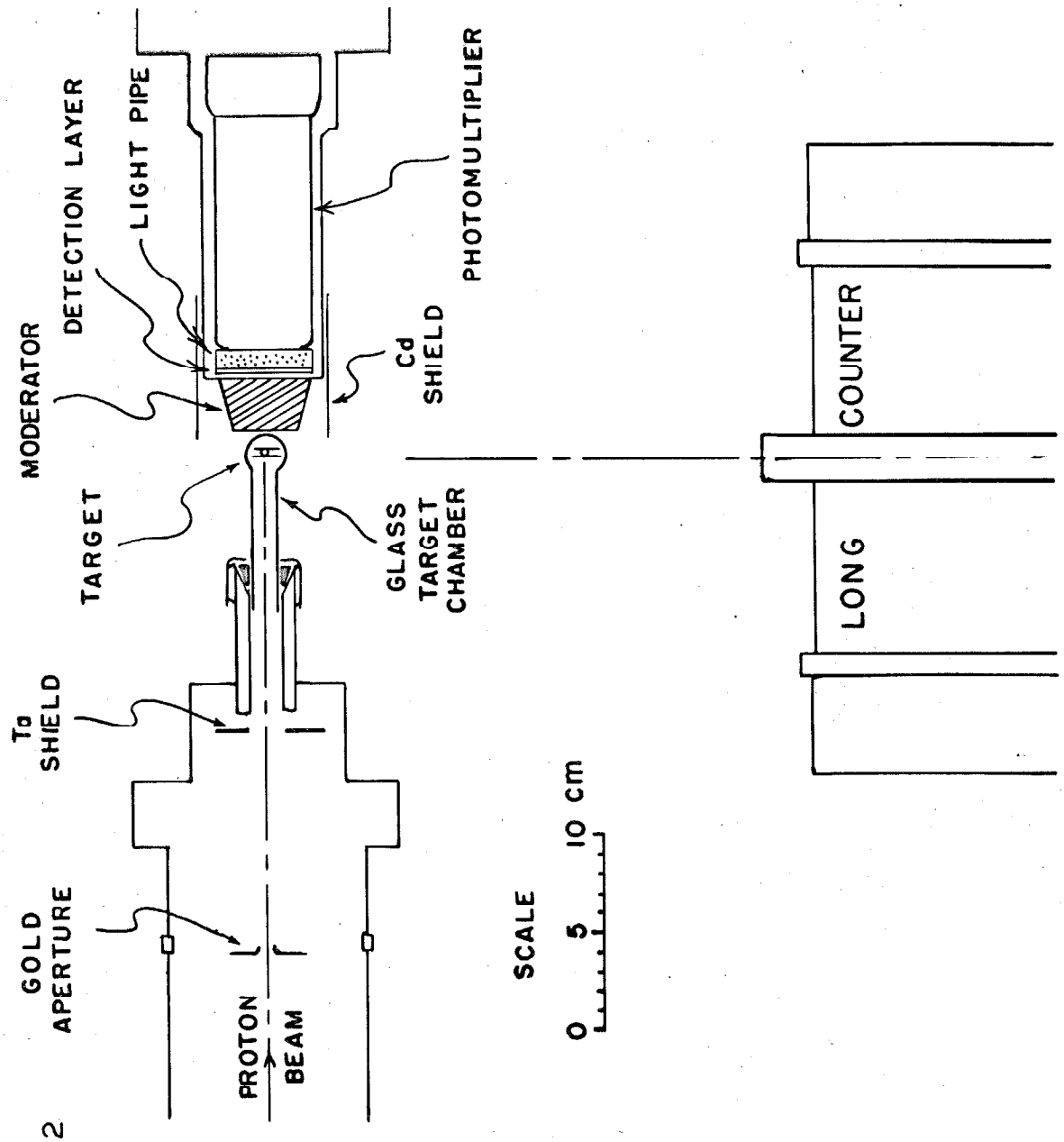
MODERATOR
DETECTION LAYER
LIGHT PIPE
PHOTOMULTIPLIER
Cd SHIELD
TARGET
GLASS TARGET CHAMBER
To SHIELD
GOLD APERTURE
PROTON BEAM
COUNTER
LONG
SCALE
0 5 10 cm

Figure 2

Figure 3. Neutron velocity diagram near threshold, drawn to scale for the $Li^6(p, n)Be^6$ reaction. The circles are loci of the end point of the laboratory neutron velocity vector, v_n, for various values of ϵ. The cone at the angle $\alpha = 58^o$ is defined by the edge of the moderator with respect to the target spot. The locus for ϵ_α shows the neutron cone matching the moderator cone. The neutron cone opens to 180^o at ϵ_π. See pp. 17, 18, 45-47.

Figure 3

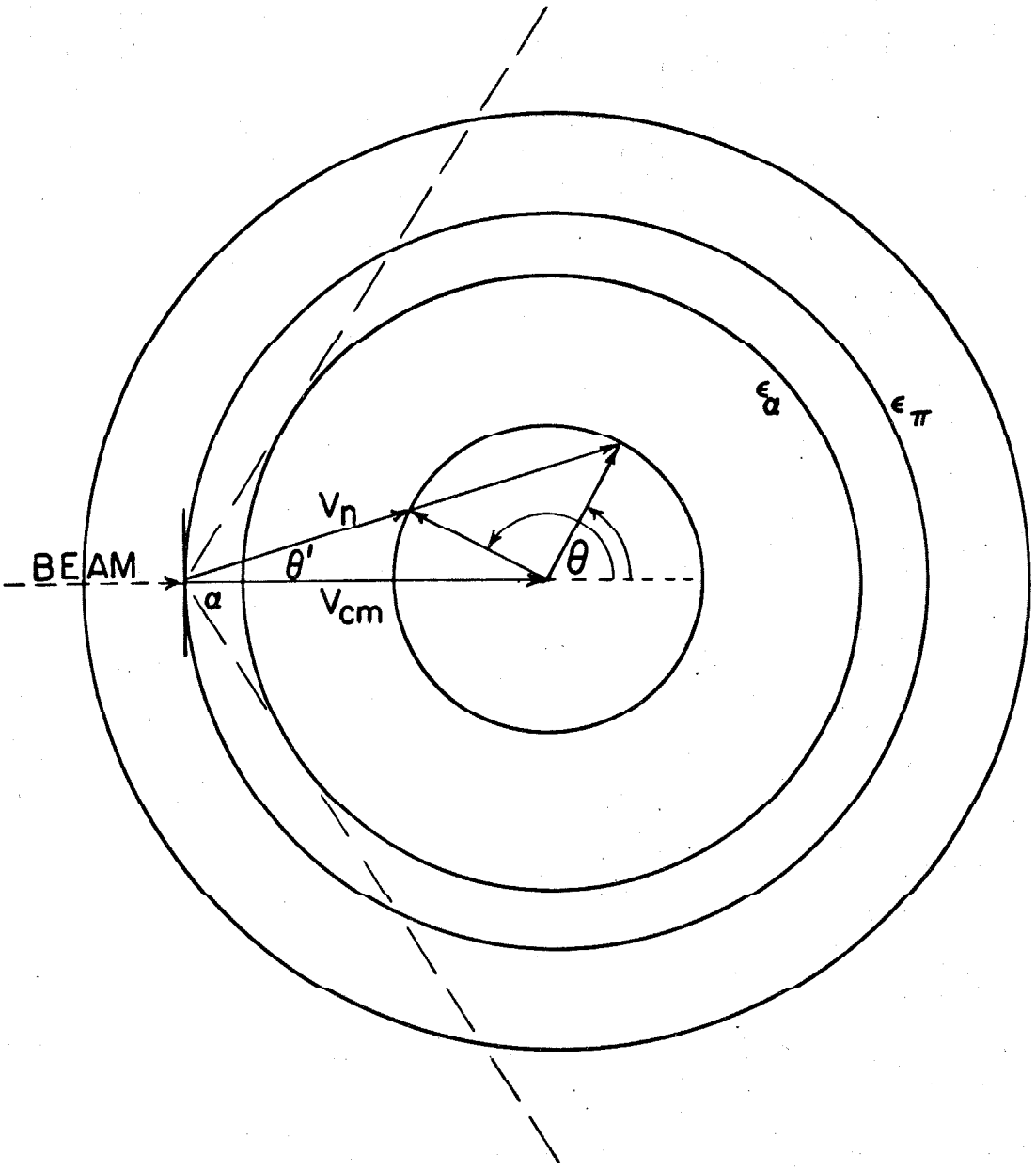

Figure 4. The detector response function. Results from the Monte Carlo calculation using the $Li^6(p, n)Be^6$ kinematics are shown as points. The lines indicate the power-law approximation used in the data analysis. See pp. 19, 27, 45-48.

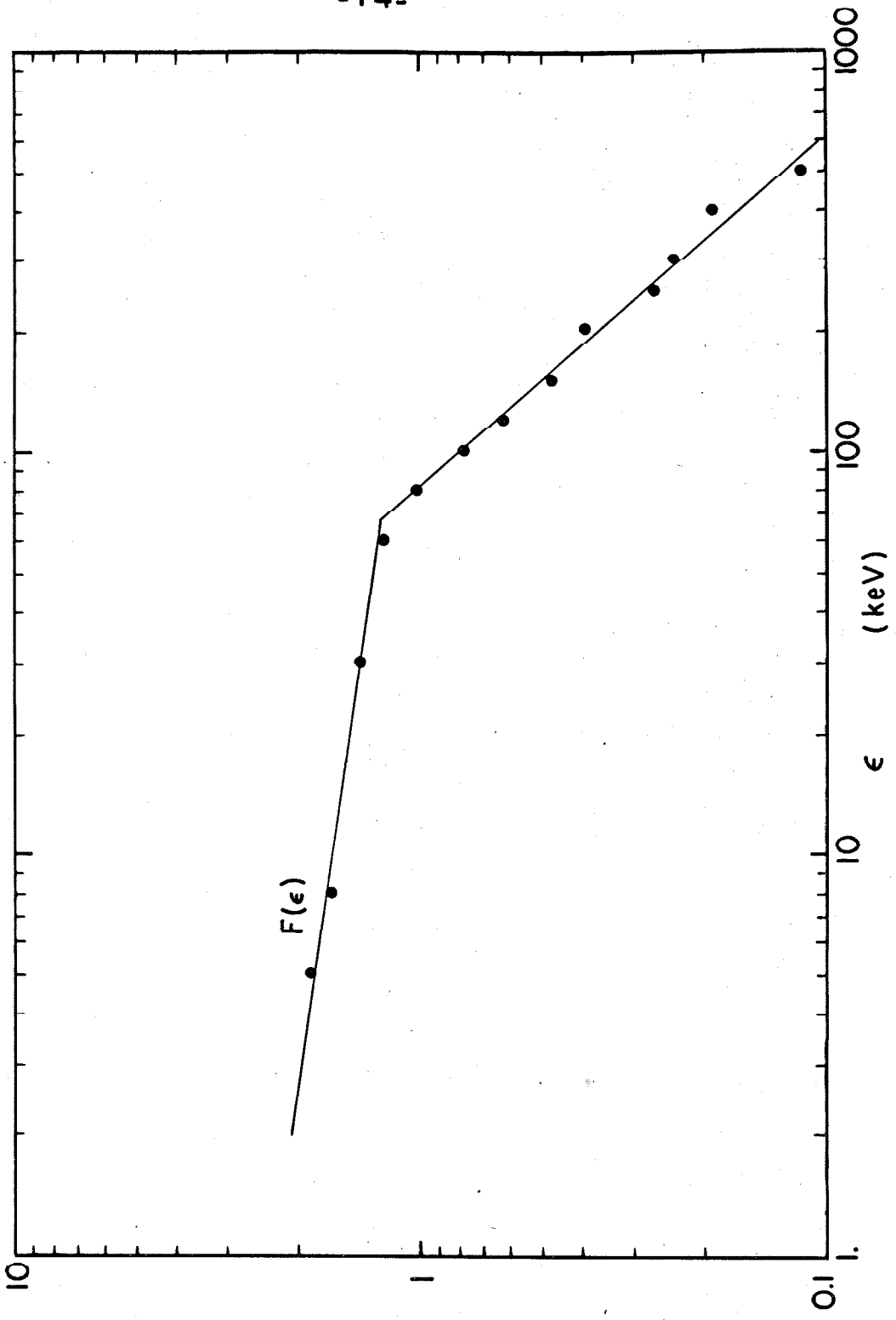

Figure 4

Figure 5. Disposition of neutrons according to the Monte Carlo calculation for the $Li^6(p, n)Be^6$ reaction. The neutrons which do not intercept the detector are grouped according to those which are emitted outside of the moderator cone, those which scatter out of the moderator to the side or front, and those which pass through the moderator but outside the disk of the detector. The rest of the neutrons have a probability of being detected which follows the 1/v law. Their energy groups are lettered as in Table I. See pp. 19, 20, 47.

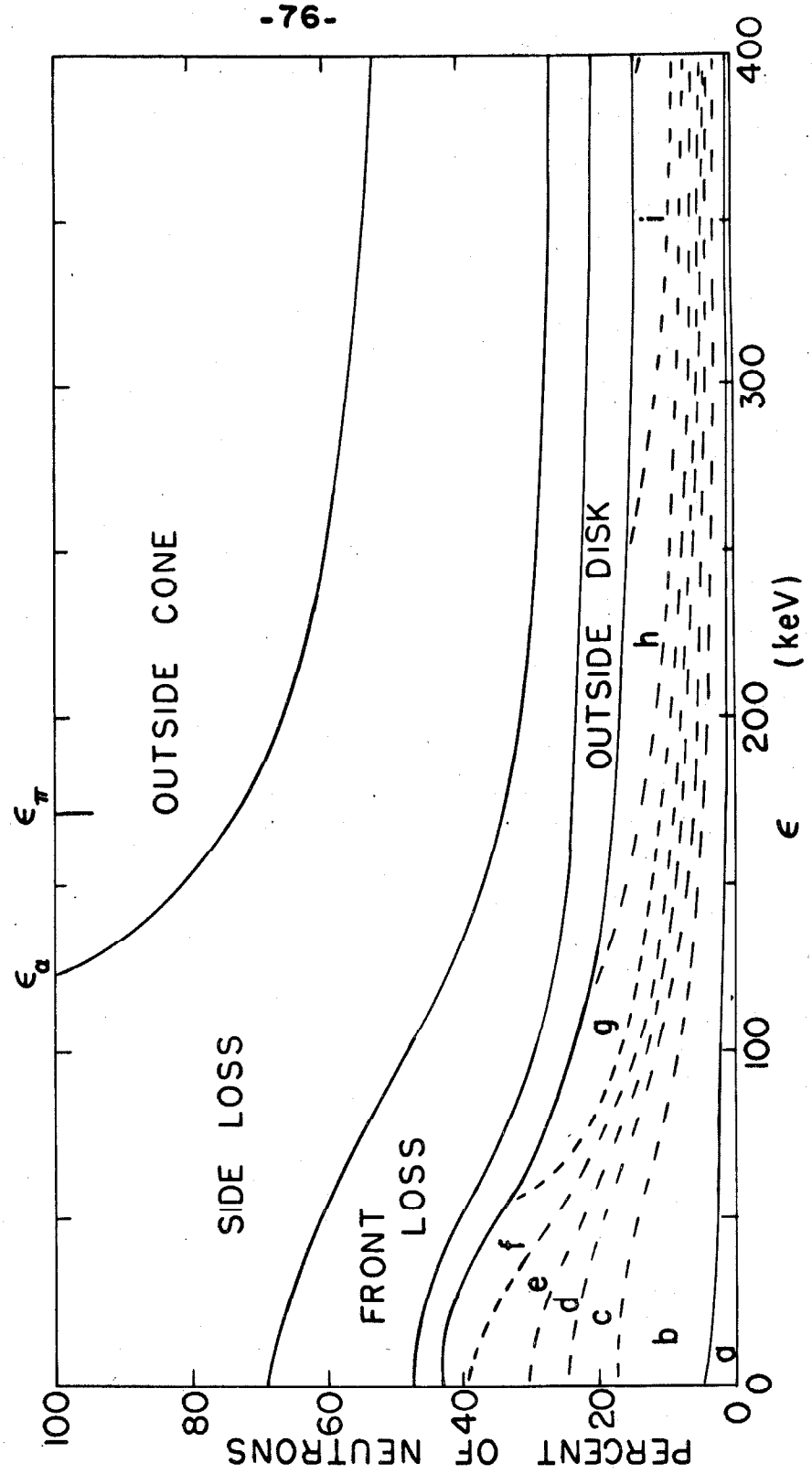
OUTSIDE CONE
SIDE LOSS
FRONT LOSS
OUTSIDE DISK
ϵ_a
ϵ_π
a
b
c
d
e
f
g
h
i
PERCENT OF NEUTRONS
100
80
60
40
20
0
0
100
200
300
400
ϵ (keV)

Figure 5

Figure 6. Data from the threshold detection system after subtraction of the gold background. The target material, enriched or natural lithium, is shown at the left of the corresponding curve. The logarithmic vertical scale is arbitrary. The method of normalizing the curves for subtraction to isolate the Li^6 contribution is indicated by the dashed line. See pp. 21, 22, 34.

Figure 6

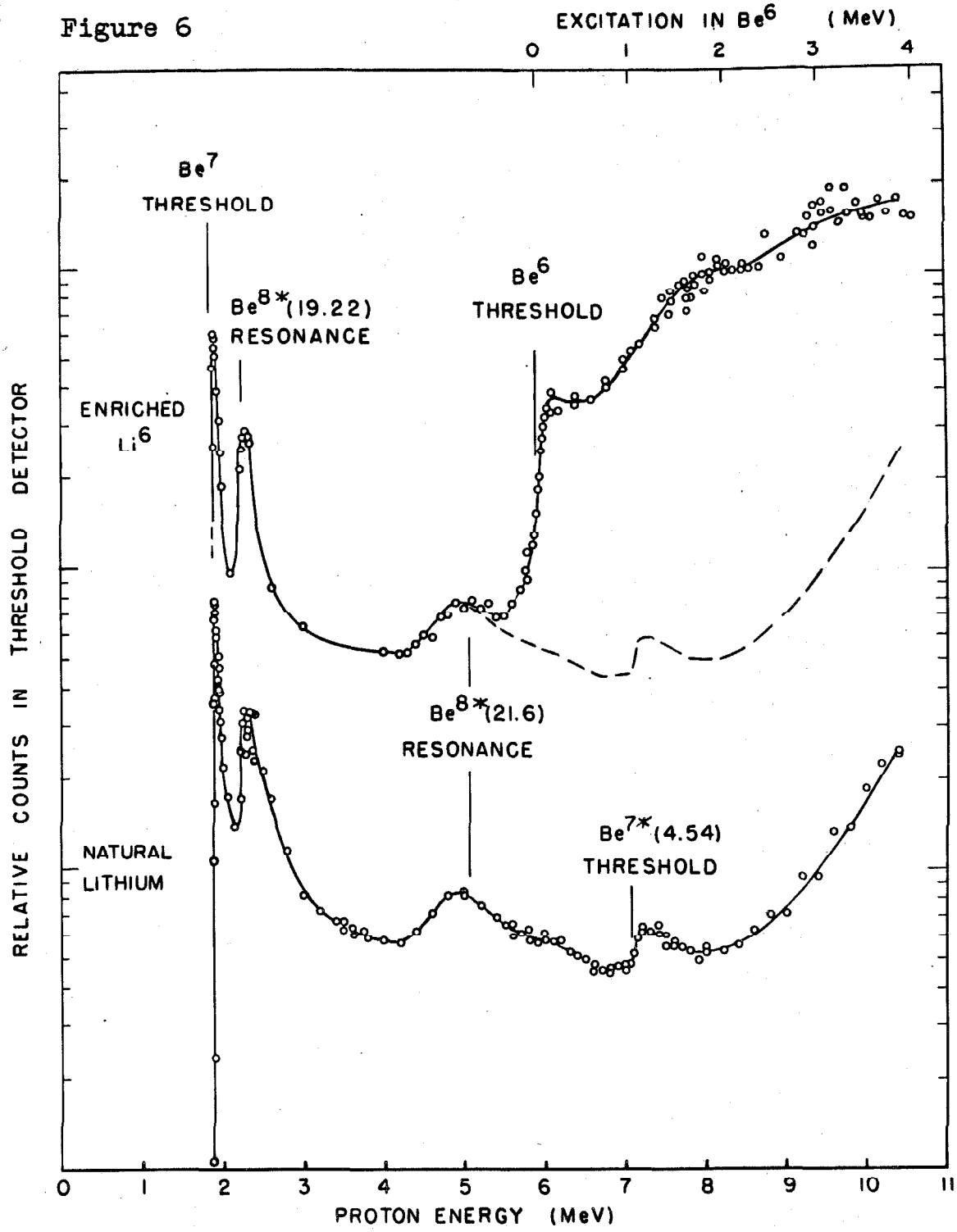
EXCITATION IN Be6 (MeV)
0
1
2
3
4
Be7
THRESHOLD
Be8*(19.22)
RESONANCE
Be6
THRESHOLD
ENRICHED
Li6
Be8*(21.6)
RESONANCE
Be7*(4.54)
THRESHOLD
NATURAL
LITHIUM
RELATIVE COUNTS IN THRESHOLD DETECTOR
0
1
2
3
4
5
6
7
8
9
10
11
PROTON ENERGY (MeV)

Figure 7. Reduced data from the threshold detector at the Be^6 threshold. (a) The three curves fit to the data points correspond to central values of the parameters as plotted in Figure 11. (b) The base line was shifted upward by 202 counts to obtain the fit shown. With the base line shifted 307 counts, a Li^5 + p curve nearly indistinguishable from this one was obtained, but the parameters were E_{th} = 5.930 MeV and Γ_0 = 0.105 MeV. These last two cases are plotted in Figure 12. See pp. 22, 31, 32; Table III.

Figure 7

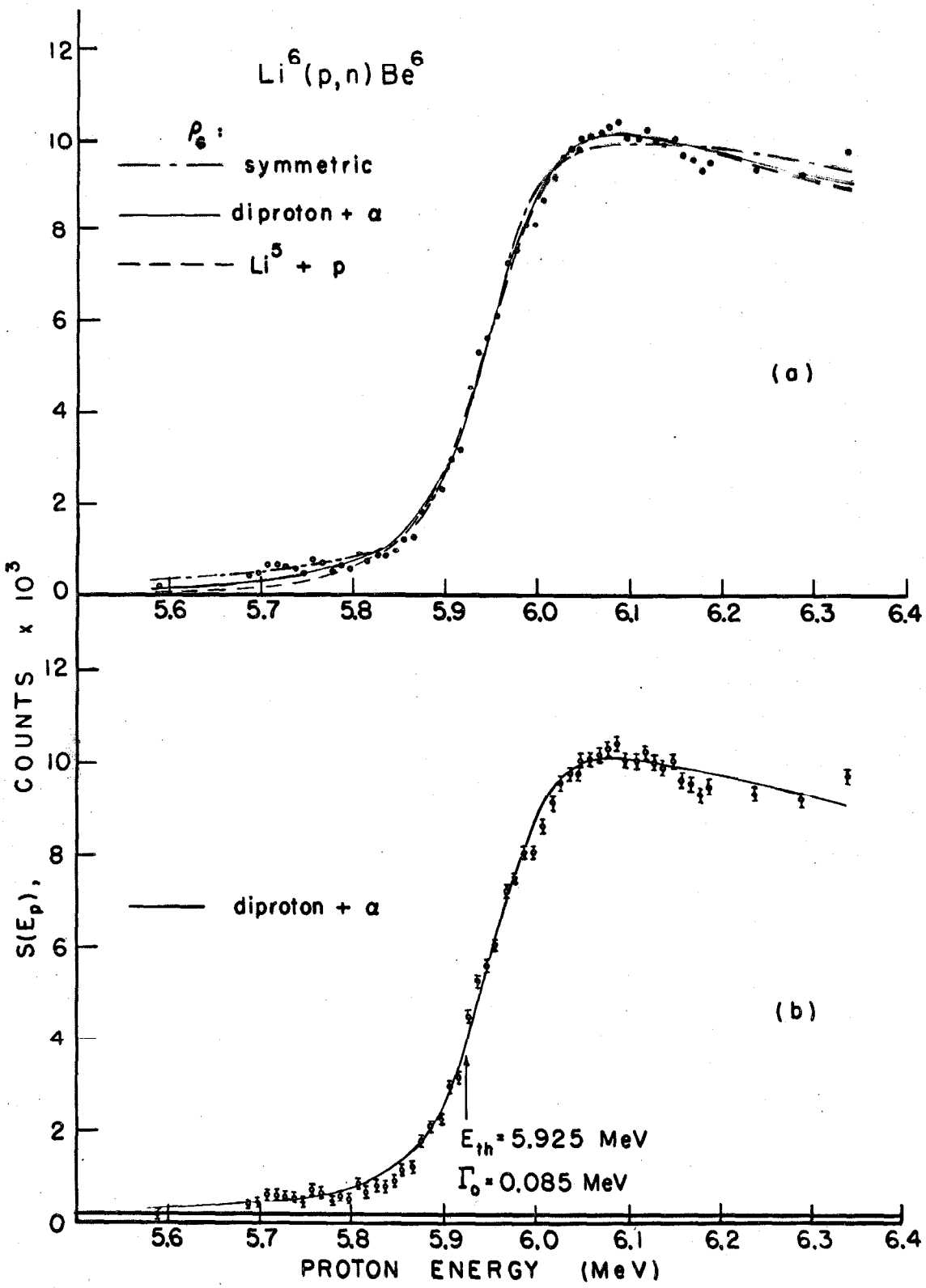
$Li^6(p,n)Be^6$
ρ_θ :
symmetric
diproton + α
Li^5 + p
(a)
diproton + α
(b)
E_{th} = 5.925 MeV
Γ_0 = 0.085 MeV
$S(E_p)$, COUNTS x 10^3
PROTON ENERGY (MeV)
0
2
4
6
8
10
12
5.6
5.7
5.8
5.9
6.0
6.1
6.2
6.3
6.4

Figure 8. Target thickness estimation at the $Li^7(p, n)Be^7$ threshold. The target was the one from which the data in Figure 10 were obtained. The energy loss of protons in the target layer cannot exceed the 25 keV difference between the threshold and the peak of the curve. See p. 23.

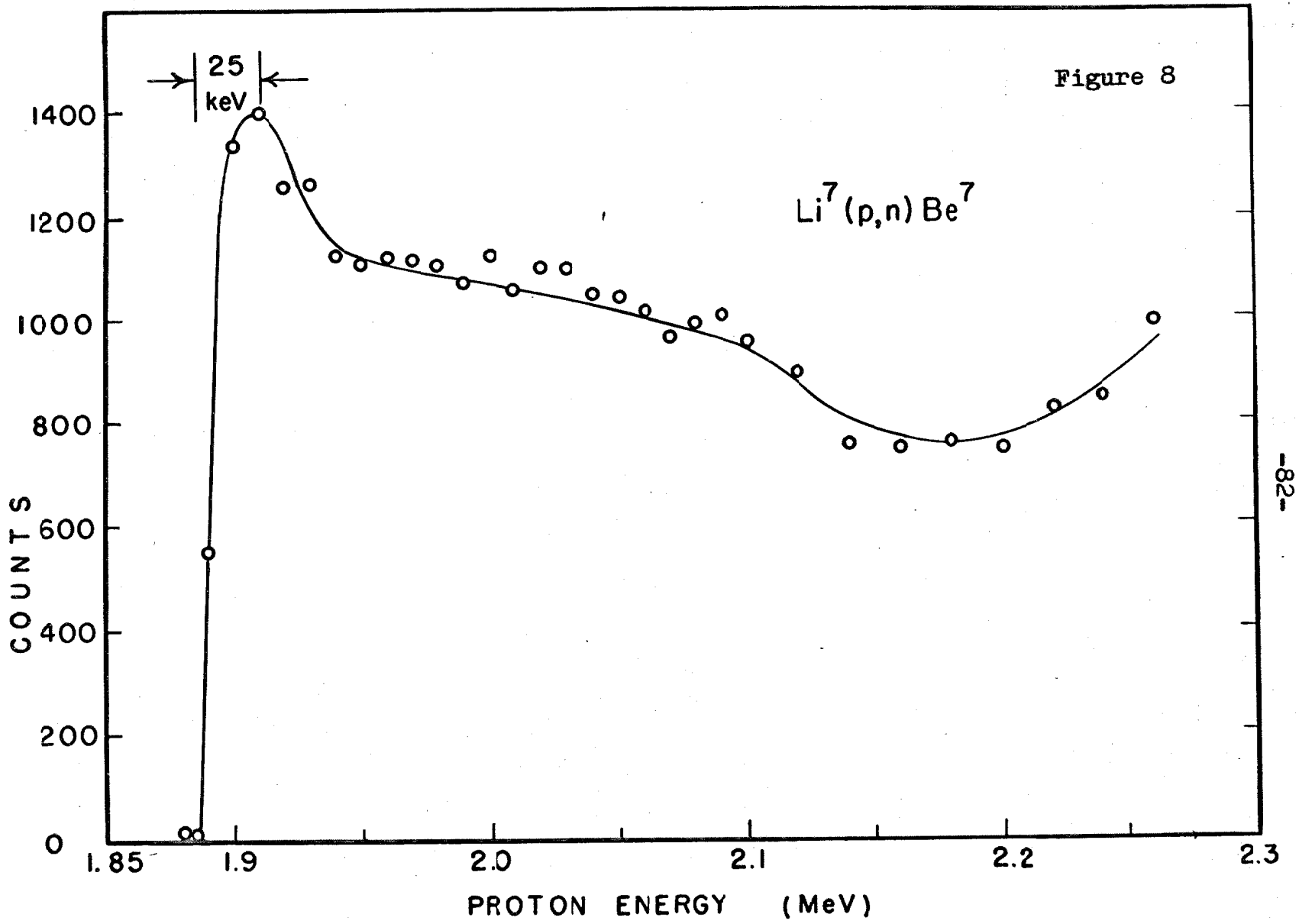
25
keV
Figure 8
$Li^7(p,n)Be^7$
COUNTS
0
200
400
600
800
1000
1200
1400
1.85
1.9
2.0
2.1
2.2
2.3
PROTON ENERGY (MeV)

Figure 9. Density of states and width functions for the diproton + α decay of Be^6. ρ_2 is obtained from the proton-proton effective range parameters. The Be^6 density of states ρ_6 and width Γ have been calculated from ρ_2. The densities of states are multiplied by an arbitrary factor. See pp. 29, 30, 52, 53.

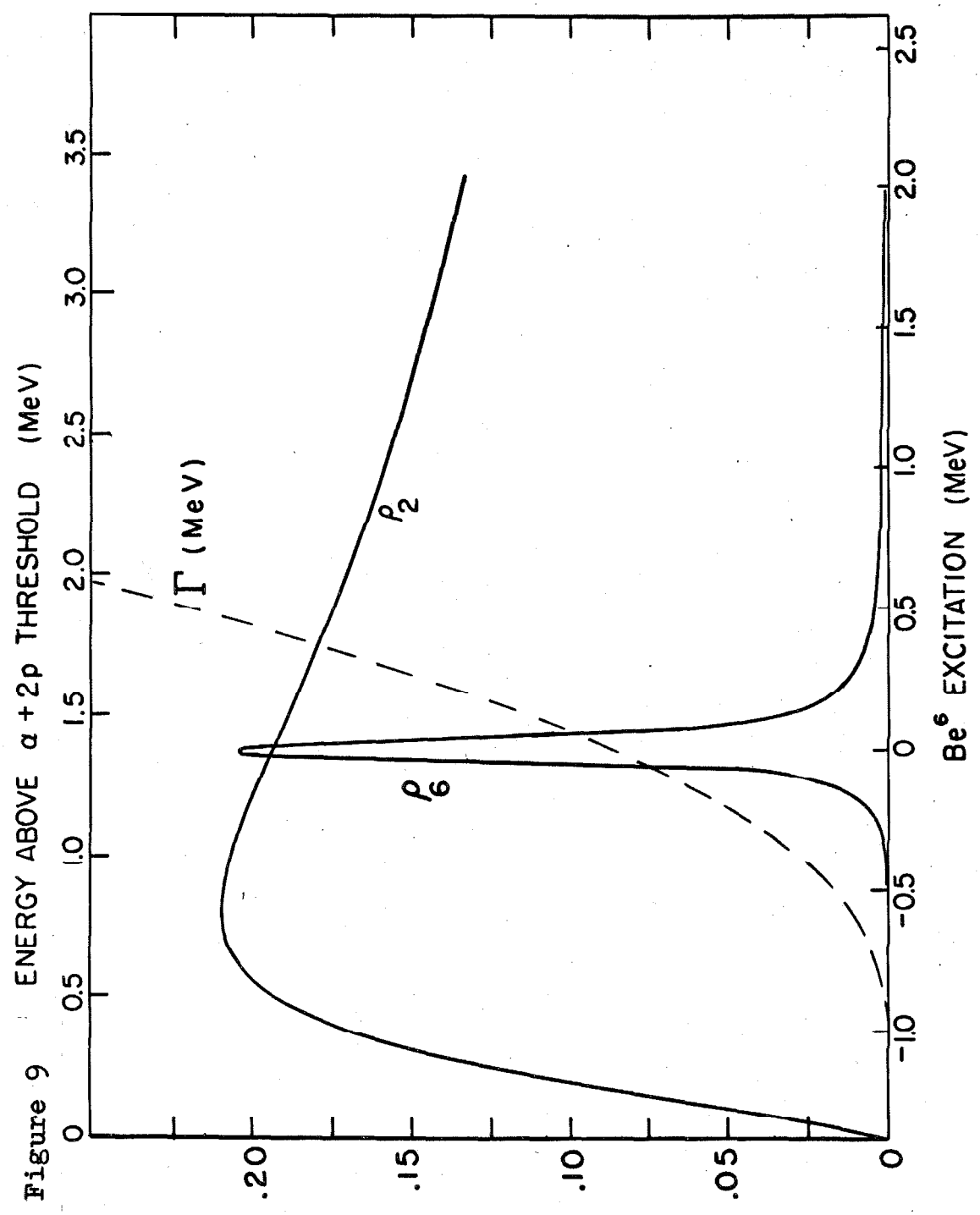
ENERGY ABOVE α + 2p THRESHOLD (MeV)
Be⁶ EXCITATION (MeV)
Γ (MeV)
ρ2
ρ6
0
.05
.10
.15
.20
0.5
1.0
1.5
2.0
2.5
3.0
3.5
-1.0
-0.5
0
0.5
1.0
1.5
2.0
2.5

Figure 9

Figure 10. Density of states and width functions for the Li^5 + p decay of Be^6. P + α scattering results for the Li^5 ground-state resonance were used to calculate ρ_5. This was used in turn to obtain the Be^6 density of states ρ_6 and width Γ. The densities of states are multiplied by an arbitrary factor. See pp. 30, 31, 52, 53.

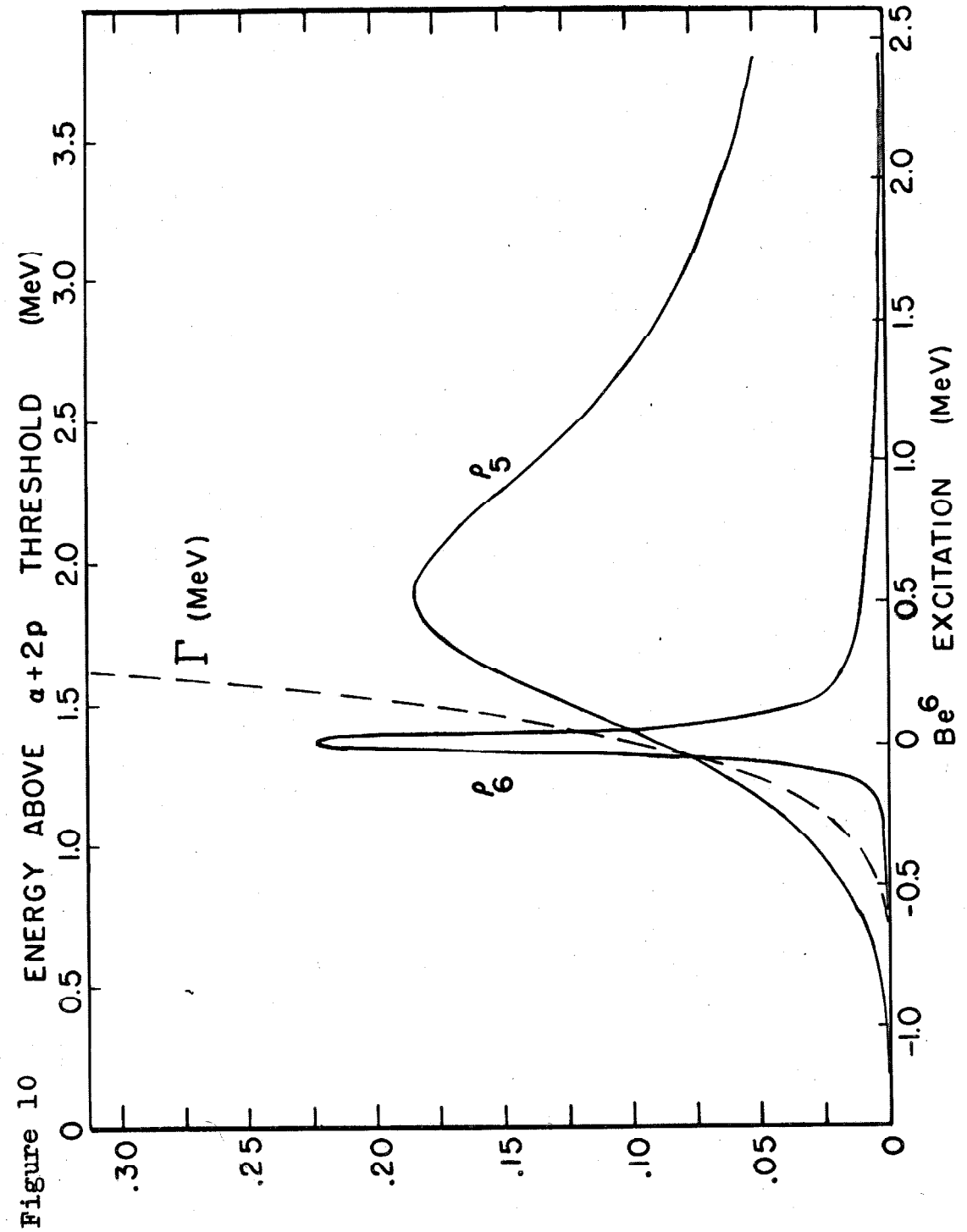
ENERGY ABOVE α+2p THRESHOLD (MeV)
0
0.5
1.0
1.5
2.0
2.5
3.0
3.5
Γ (MeV)
.30
.25
.20
.15
.10
.05
0
ρ5
ρ6
Be6 EXCITATION (MeV)
2.5
2.0
1.5
1.0
0.5
0
-0.5
-1.0

Figure 10

Figure 11. Standard deviation contours for fits with fixed base line. Examples of these fits are shown in Figure 7a. The label for each contour indicates the decay mode of the density of states function ρ_6 which was assumed. The probability that the correct values lie outside of the contour is the same as that for a single parameter to be more than one standard deviation away from its measured value. The orientation of the elongated contours with respect to the axes indicated correlation between the parameters in the fit. The triangles are the least-squares adjusted values which required the minimum adjustment from the lattice of all fits which were made. For the Li^5 + p case, the effect of varying the response function is shown. The "T" mark is the result for the best fit using ϵ_b = 30 keV, and the "L" mark is the result using ϵ_b = 123 keV. Probable errors obtained from these are discussed in the text. See pp. 31, 32, 33, 40.

Figure 11

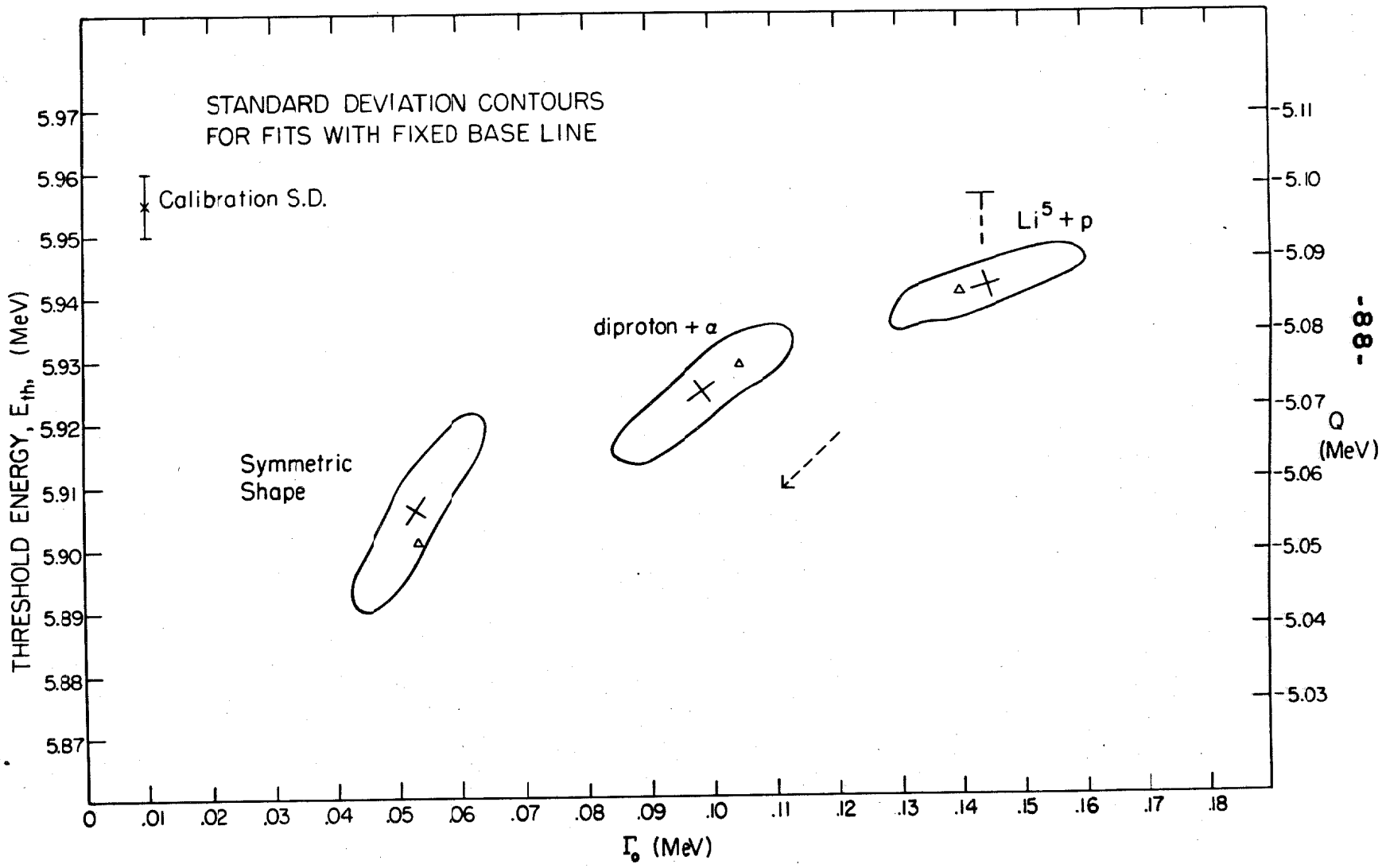
STANDARD DEVIATION CONTOURS
FOR FITS WITH FIXED BASE LINE
Calibration S.D.
Li5 + p
diproton + α
Symmetric
Shape
THRESHOLD ENERGY, Eth. (MeV)
5.97
5.96
5.95
5.94
5.93
5.92
5.91
5.90
5.89
5.88
5.87
5.11
5.10
5.09
5.08
5.07
5.06
5.05
5.04
5.03
Q
(MeV)
0
.01
.02
.03
.04
.05
.06
.07
.08
.09
.10
.11
.12
.13
.14
.15
.16
.17
.18
Γo (MeV)

Figure 12. Standard deviation contours for fits with adjusted base line. The diproton + α case is illustrated in Figure 7b. The symbols are discussed in connection with Figure 11. The "L" mark corresponds to ϵ_b = 123 keV for the diproton + α case. The result of Whaling (1964) from the $Li^6(He^3, t)Be^6$ reaction has been converted into the quantities plotted in this figure and shown for comparison. Correction for the distortion of ρ_6 for both decay modes has been made in the latter contour. See pp. 32, 33, 40, 41, 43.

Figure 12

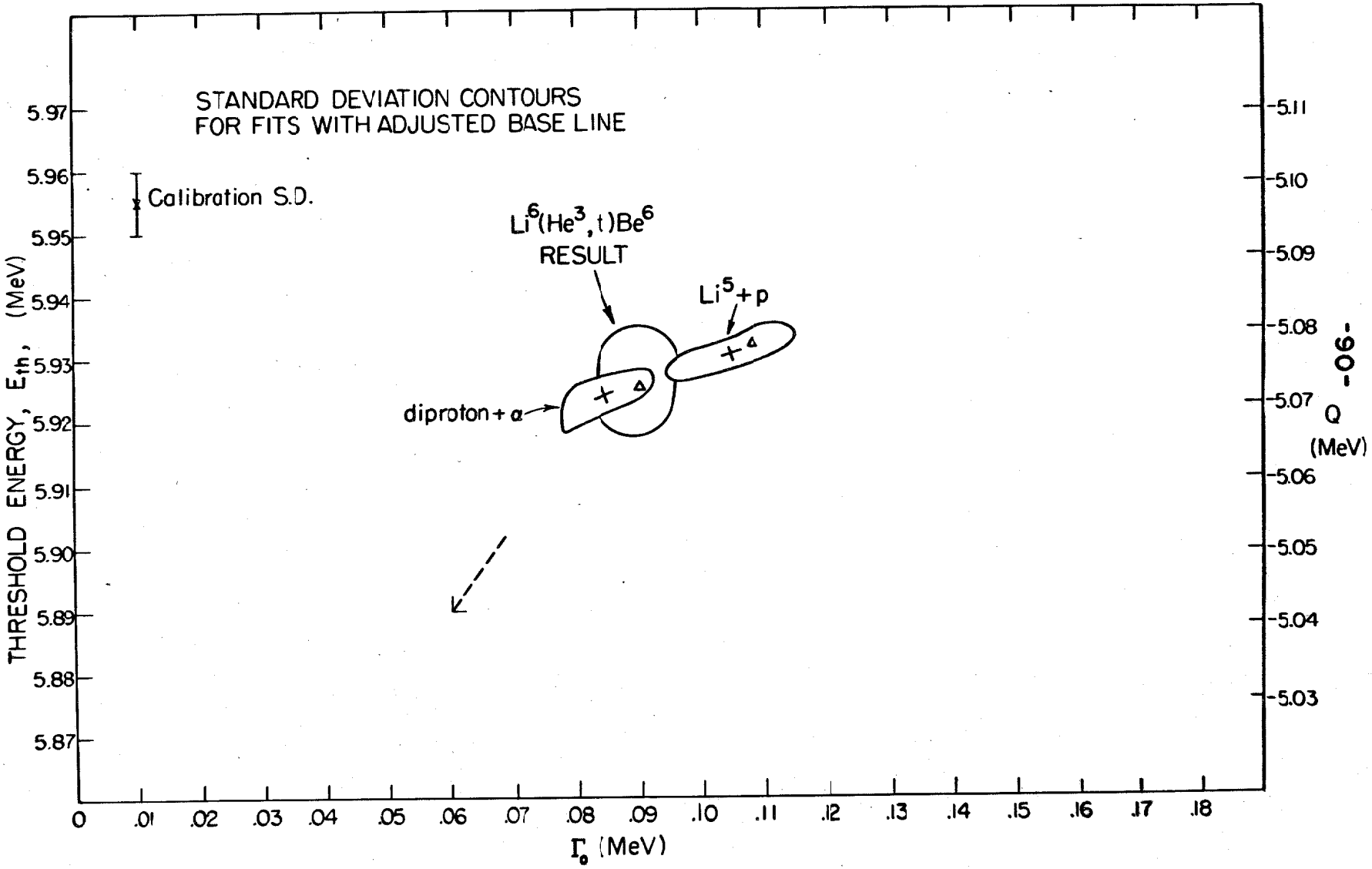
STANDARD DEVIATION CONTOURS
FOR FITS WITH ADJUSTED BASE LINE
Calibration S.D.
$Li^6(He^3,t)Be^6$
RESULT
Li^5+p
diproton + α
THRESHOLD ENERGY, E_{th}, (MeV)
5.97
5.96
5.95
5.94
5.93
5.92
5.91
5.90
5.89
5.88
5.87
-5.11
-5.10
-5.09
-5.08
-5.07
-5.06
-5.05
-5.04
-5.03
Q (MeV)
0
.01
.02
.03
.04
.05
.06
.07
.08
.09
.10
.11
.12
.13
.14
.15
.16
.17
.18
Γ_0 (MeV)

Figure 13. Data from the long counter after subtraction of the gold background. The target material for each curve is shown at the left. The normalization for the purpose of estimating the (p, n) cross section of Li^6 from that of Li^7 is indicated by the dashed line. The logarithmic vertical scale is arbitrary. See p. 35.

Figure 13

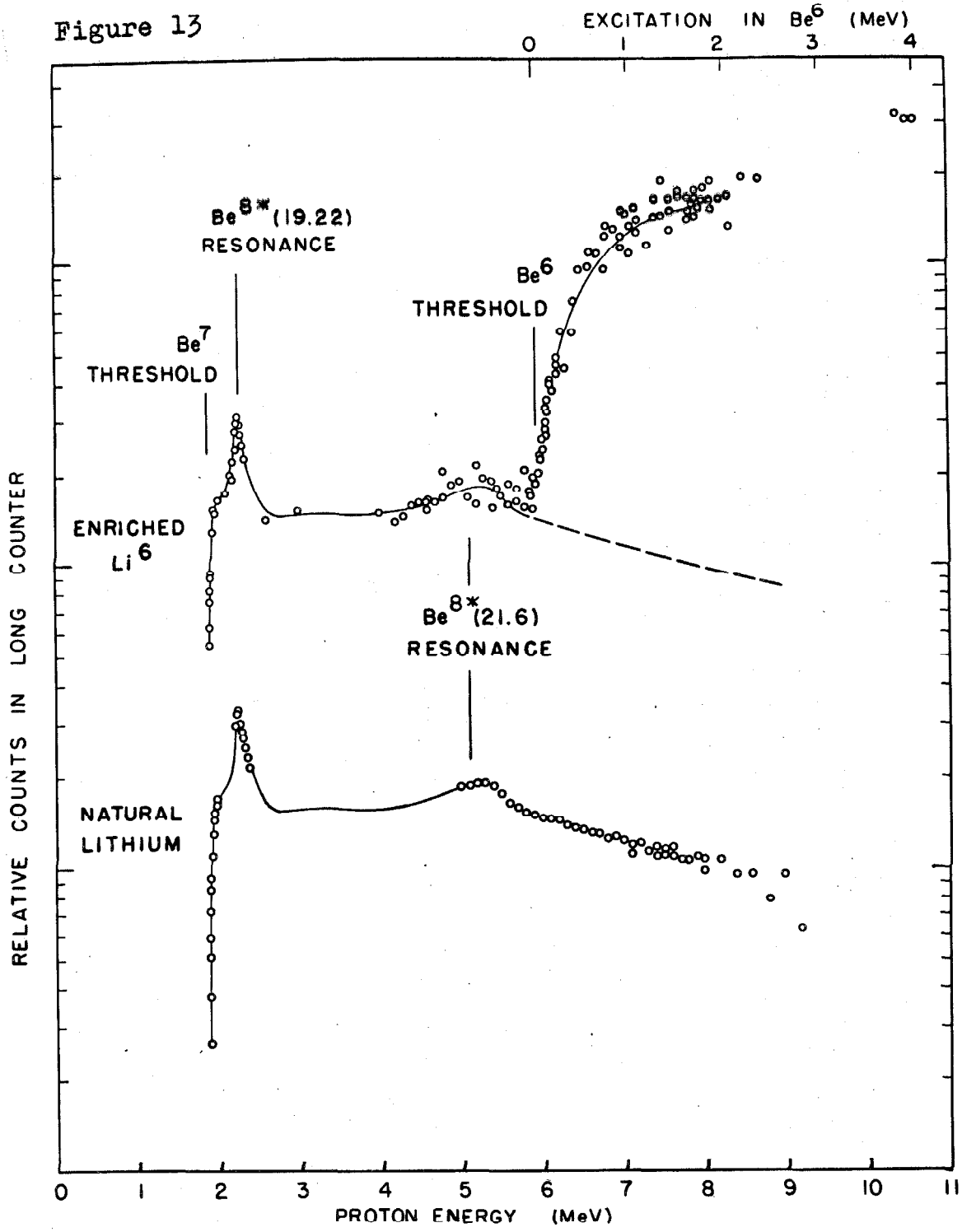
EXCITATION IN Be6 (MeV)
0
1
2
3
4
Be8* (19.22)
RESONANCE
Be6
THRESHOLD
Be7
THRESHOLD
ENRICHED
Li6
Be8* (21.6)
RESONANCE
NATURAL
LITHIUM
RELATIVE COUNTS IN LONG COUNTER
0
1
2
3
4
5
6
7
8
9
10
11
PROTON ENERGY (MeV)

Figure 14. Differential cross section at 90° in the laboratory for neutron production from Li^6 + p. The magnitude of the cross section was estimated by comparison with the $Li^7(p, n)Be^7$ reaction. The dashed lines indicate probable errors. The point A shows the result of Ajzenberg-Selove et al., (1959) for the Be^6 ground-state neutron group. The lower part of the curve was calculated using the parameters measured with the threshold detector, folded with a flat response function and fit to the data curve between 6.0 and 6.6 MeV. See pp. 36, 37, 39.

Figure 14

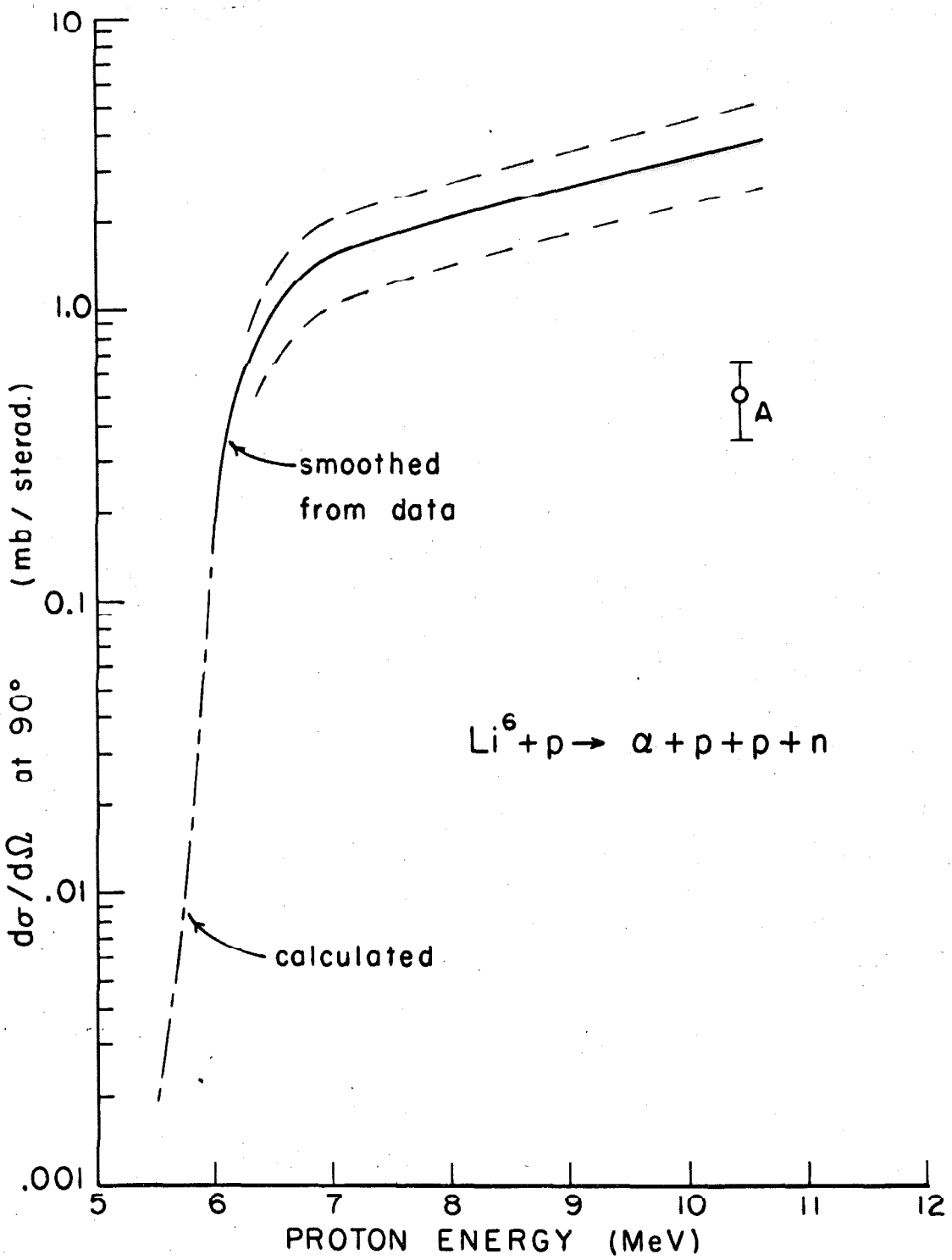
10
1.0
0.1
.01
.001
dσ/dΩ at 90° (mb / sterad.)
smoothed
from data
calculated
A
Li⁶ + p → α + p + p + n
5
6
7
8
9
10
11
12
PROTON ENERGY (MeV)

Figure 15. The calculated $Li^6(p, n)Be^6$ excitation function. The parameters obtained from the diproton + α fit were used and the detector response function was replaced with a constant in Equation (IV. 2). This corresponds to measuring the neutrons at all angles, hence, the result is proportional to the total cross section. The same calculation is used for the lower part of the curve in Figure 14. See p. 39.

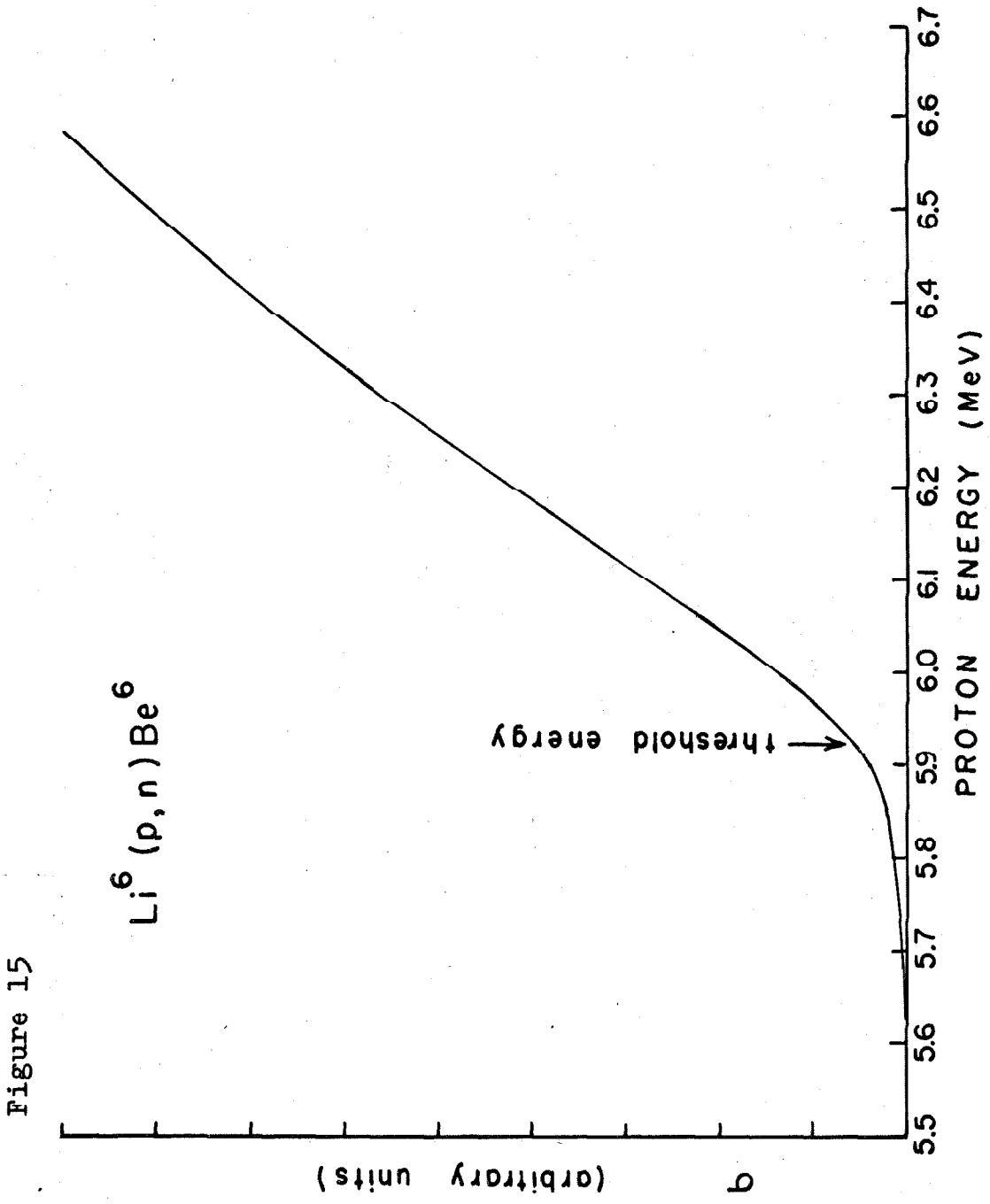
$Li^6(p,n)Be^6$
threshold energy
q (arbitrary units)
5.5
5.6
5.7
5.8
5.9
6.0
6.1
6.2
6.3
6.4
6.5
6.6
6.7
PROTON ENERGY (MeV)

Figure 15

Figure 16. (a) The detector response function calculated for the reaction $Li^7(\alpha, n)B^{10}$. The Monte Carlo points and power law approximation are shown as in Figure 4. (b) Measurements above the $Li^7(\alpha, n)B^{10}$ threshold compared with the response function multiplied by s- and p-wave penetration factors. See pp. 50, 51.

Figure 16

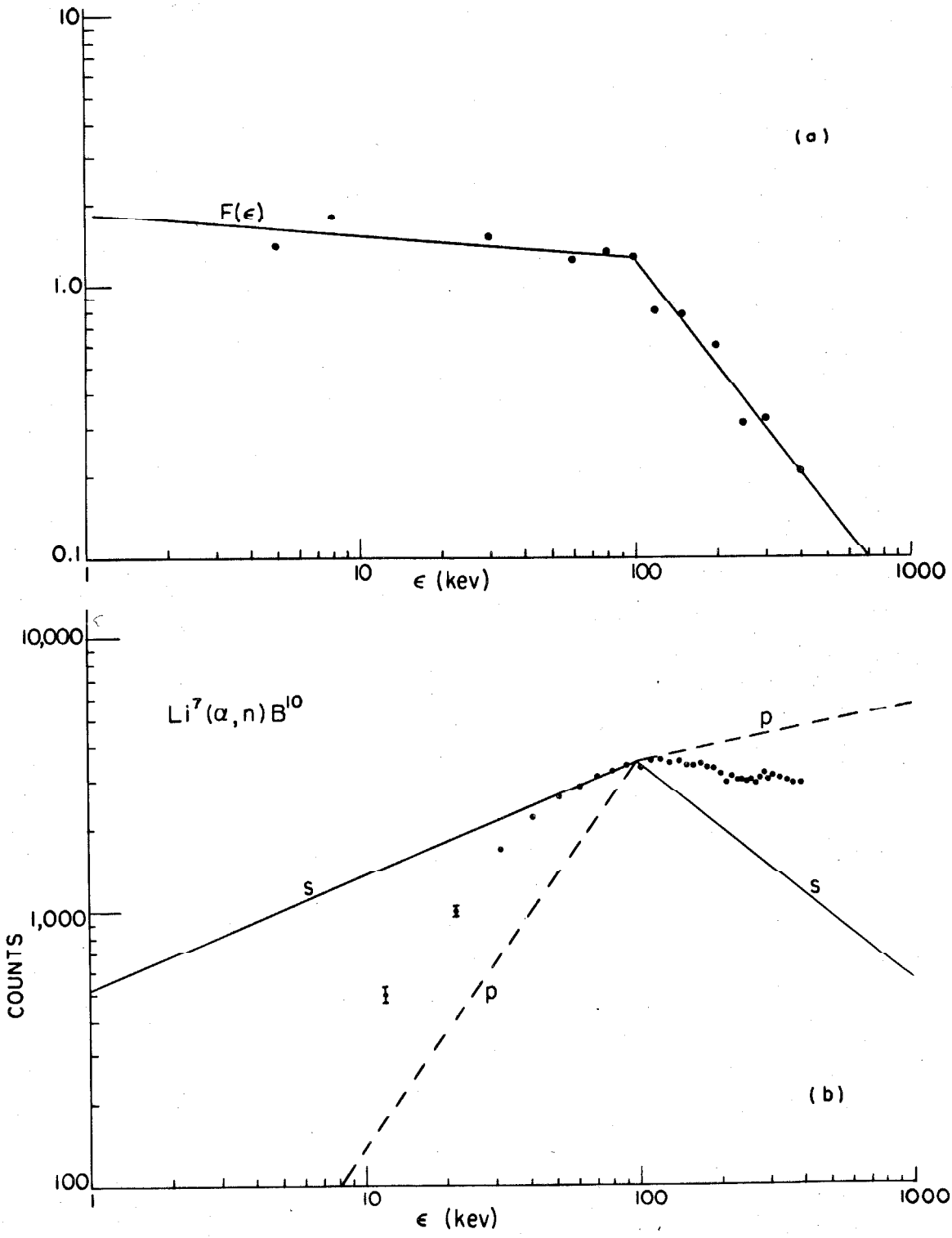
10
1.0
0.1
F(ϵ)
(a)
1
10
100
1000
ϵ (kev)
10,000
1,000
100
COUNTS
Li⁷(α,n)B¹⁰
p
s
s
p
(b)
1
10
100
1000
ϵ (kev)